Analytic theory of high-order-harmonic generation by an intense few-cycle laser pulse

M. V. Frolov, N. L. Manakov, A. M. Popov, O. V. Tikhonova, E. A. Volkova, A. A. Silaev, N. V. Vvedenskii, and Anthony F. Starace

Phys. Rev. A **85**, 033416 — Published 13 March 2012

DOI: 10.1103/PhysRevA.85.033416

Analytic Theory of High-Order Harmonic Generation by an Intense Few-Cycle Laser Pulse

M. V. Frolov and N. L. Manakov
Department of Physics, Voronezh State University, Voronezh 394006, Russia

A. M. Popov, O. V. Tikhonova, and E. A. Volkova
D.V. Skobeltsyn Institute of Nuclear Physics, M.V. Lomonosov Moscow State University, Moscow 199991, Russia

A. A. Silaev and N. V. Vvedenskii
Institute of Applied Physics, Russian Academy of Sciences, Nizhny Novgorod 603950, Russia

Anthony F. Starace
Department of Physics and Astronomy, The University of Nebraska, Lincoln NE 68588-0299, USA

We present a theoretical model for describing the interaction of an electron, weakly bound in a short-range potential, with an intense, few-cycle laser pulse. General definitions for the differential probability of above threshold ionization and for the yield of high-order harmonic generation (HHG) are presented. For HHG we then derive detailed analytic expressions for the spectral density of generated radiation in terms of the key laser parameters, including the number, N, of optical cycles in the pulse and the carrier-envelope phase (CEP). In particular, in the tunneling approximation, we provide detailed derivations of the closed-form formulas presented briefly by M.V. Frolov *et al.* [Phys. Rev. A **83**, 021405(R) (2011)], which were used to describe key features of HHG by both H and Xe atom targets in an intense, few-cycle laser pulse. We then provide a complete analysis of the dependence of the HHG spectrum on both N and the CEP ϕ of an N-cycle laser pulse. Most importantly, we show analytically that the structure of the HHG spectrum stems from interference between electron wave packets originating from electron ionization from neighboring half-cycles near the peak of the intensity envelope of the few-cycle laser pulse. Such interference is shown to be very sensitive to the CEP. The usual HHG spectrum for a monochromatic driving laser field (comprising harmonic peaks at odd multiples of the carrier frequency and spaced by twice the carrier frequency) is shown analytically to occur only in the limit of very large N, and begins to form, as N increases, in the energy region beyond the HHG plateau cutoff.

PACS numbers: 42.65.Ky, 32.80.Rm

I. INTRODUCTION

The high-order harmonic generation (HHG) process is now the major means for producing ultrashort pulses in the rapidly-developing field of attosecond physics (cf. recent reviews [1–5]) as well as for producing coherent radiation in the soft x-ray regime [6]. At present it is possible experimentally to obtain HHG spectra using short (few cycle) laser pulses [2, 7–9]. The short-pulse HHG spectra are highly sensitive to the temporal behavior of the electric field of the laser pulse, i.e., to the shape of the pulse envelope, $f(t)$, and the carrier-envelope phase (CEP), ϕ. For laser parameters in the tunneling regime, the three-step scenario [10, 11] remains applicable for understanding some basic features of HHG by atoms in a short laser pulse. However, there are at least two important differences from the monochromatic field case. First, the HHG emission becomes quasi-continuous, so that instead of analyzing HHG rates it is more appropriate to analyze the spectral density of radiation, $\rho(E_\Omega)$, where $E_\Omega = \hbar\Omega$ is the harmonic photon energy. Second, the shape of $\rho(E_\Omega)$ as a function of E_Ω for a rapidly-varying laser pulse envelope becomes sensitive to the CEP, requiring an analysis of subcycle dynamics for a proper description.

From 1998 up to the present, the key differences between short-pulse and monochromatic field HHG spectra have been delineated in numerous theoretical and experimental investigations [12–23]. The most significant differences were found in the shape and the plateau-cutoff behavior of HHG spectra for "sine" ($\phi = \pi/2$) and "cosine" ($\phi = 0$) pulses. Nearly all of the theoretical analyses of few-cycle pulse HHG spectra are based on numerical solutions of the time-dependent Schrödinger equation (TDSE) [12, 14, 15, 19, 20] or on the use of the Lewenstein *et al.* model [24] and its modifications. Recently, however, a closed-form formula for the spectral density of radiation, $\rho(E_\Omega)$, was presented [22], thus providing an analytic description of the short-pulse HHG spectrum similar to that for a monochromatic field [25].

A key feature of the closed-form analytic formula presented in Ref. [22] is that it confirms the validity for the case of a few-cycle pulse of the phenomenological parametrization [26–28] of the HHG yield in terms of the photorecombination cross section (PRCS) $\sigma^{(r)}$ (which describes the final step of the three-step scenario) and the "electron wave packet" (EWP) (which describes the ionization of an atomic electron and its propagation in the laser field). This parametrization is attractive since (i)

it is valid for harmonics with energies in the region of the HHG plateau cutoff, which are precisely the ones used to produce attosecond pulses, and (ii) it involves a field-free atomic parameter $\sigma^{(r)}$ that describes atomic structure effects on HHG spectra [25–32]. Furthermore, the explicit form of the EWP is now known not only for monochromatic [25] and two-color [31] fields, but also for the case of a few-cycle laser pulse [22]. Consequently, the closed-form formula for the short-pulse case in Ref. [22] makes possible the analytic exploration of many-electron atomic features in the HHG spectrum and their modification by CEP effects. As shown in Ref. [22], all that is required is the PRCS $\sigma^{(r)}$ for the target atom and the solutions of some classical equations for a given short laser pulse. Results of the analytic formula for the HHG yield in the few-cycle laser pulse case agree well with numerical TDSE results. Also, the dependence on the number of cycles, N, in the laser pulse was shown in Ref. [22] to reduce, for large N, to the analytic formula for the HHG rate in the monochromatic field case [25].

The purpose of this paper is to present the theory upon which the analytic predictions in Ref. [22] (for HHG by H and Xe atom targets driven by a few-cycle laser pulse) are based. By way of background, we note that our focus over much of the past decade has been on developing exact (and, when possible, closed-form analytic) results for a one-electron model atomic system subjected to an intense laser field. The physical insights provided by the closed-form analytic results obtained for our model system have enabled us to generalize those results to real, many-electron atomic systems and to predict many-electron effects in strong-field processes for such real systems. Thus, for example, we predicted that a giant-dipole resonance would be seen in the HHG spectrum of Xe [25]. (This prediction was subsequently confirmed by experiment [33].) Also, we were able to interpret [32] experimentally-observed resonances in particular high-order harmonics in singly-ionized plasmas of Cr^+ and Mn^+ [34, 35] as due to potential barrier effects that lead to a strong $3p \to 3d$ electric dipole transition, which dominates the many-electron photoionization cross sections of the outer subshells of those ions (as well as the corresponding PRCSs to those subshells).

The theory we have developed for our model atomic system is the time-dependent effective range (TDER) theory [36, 37]. This theory combines effective range theory (for describing a weakly bound electron in a short-range potential of arbitrary shape) with the Floquet or quasi-stationary, quasi-energy state (QQES) approach [for describing the electron's interaction with a monochromatic (or, more generally, periodic) laser field]. The TDER theory applies immediately to the case of intense laser detachment of negative ions (see, e.g., its application to laser detachment of the F^- negative ion [38], which demonstrated excellent agreement with experimental results [39]). For the HHG process, we developed a new theory applicable in general to any system interacting with a monochromatic laser field for which a Floquet or QQES approach is employed [40]. We then applied this new formulation for HHG specifically to our TDER model [41]. Based on this latter application of our new HHG formulation within TDER theory, we were able to obtain closed-form analytic formulas for HHG rates for our model system [42]. As noted above, the physical interpretation of our quantum-mechanically-derived, factorized analytic formula confirmed the well-known semiclassical three-step scenario for HHG [10, 11] and justified (for our model system) the phenomenological factorization of the HHG rate in terms of a PRCS and a EWP function [26–28]. Most importantly, the clear physical interpretation of each of the three factors in our factorized formula allowed immediate generalization for applications to HHG spectra of real atoms [25].

In this paper we present an analytic description of HHG by a short laser pulse based on two new theoretical developments. First, in Sec. II we generalize the QQES approach, which is one of the most powerful theoretical methods for accurately describing atomic processes in a strong *monochromatic laser field*, to describe the most fundamental strong field processes [i.e., above-threshold ionization (ATI) and HHG] in an intense, *few-cycle laser pulse*. Second, in Sec. III we employ this generalized QQES approach to extend our TDER theory for analytic description of HHG by a monochromatic field to the case of HHG by a periodic (non-monochromatic) pulse train field. In Sec. IV we derive the quasi-classical limit of the TDER results for the HHG amplitude in the case of a periodic (non-monochromatic) pulse train field and, as a limiting case, obtain closed-form analytic expressions for the HHG yield for the case of a single short pulse. In Sec. V we generalize our closed-form formulas to the case of real atoms. In Sec. VI we present numerical results of our analytic formulas, including comparisons with numerical TDSE results, illustrations of sub-cycle and inter-cycle interferences in short-pulse HHG spectra, and illustrations of the dependence of HHG spectra on the CEP and number of cycles in the laser pulse. In Sec.VII we summarize our results and present some conclusions. Finally, in Appendices A and B we present some of the lengthier analytic derivations of our TDER theory of HHG driven by few-cycle laser pulses.

II. GENERALIZATION OF THE QQES APPROACH TO THE CASE OF A SHORT LASER PULSE

A. Description of a Periodic Laser Pulse Train

We use the length gauge to describe the dipole interaction of an active atomic electron with a short laser pulse:

$$V(\mathbf{r}, t) = -\mathbf{d} \cdot \mathbf{F}(t), \quad \mathbf{d} = e\mathbf{r},$$

where $\mathbf{F}(t)$ is the electric vector of the pulse. Different ways are used to describe a short pulse, using either the electric vector of the pulse or its vector poten-

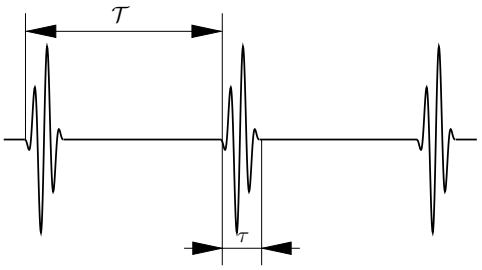

FIG. 1. Sketch of the pulse train.

tial $\mathbf{A}(t)$ [43]. In this paper, we consider only linearly-polarized pulses, so that

$$\mathbf{A}(t) = \mathbf{e}_z A(t), \tag{1}$$

$$\mathbf{F}(t) = \mathbf{e}_z F(t) = -\mathbf{e}_z \frac{1}{c}\frac{\partial A(t)}{\partial t}. \tag{2}$$

Moreover, we do not specify the explicit form of $A(t)$ in our theoretical derivations, assuming only (i) that the envelope of $A(t)$ is different from zero in the interval $(0, \tau)$ (where τ is the pulse duration) and (ii) that the shape of $A(t)$ is such that neither $\mathbf{A}(t)$ nor $\mathbf{F}(t)$ has any DC-field component. [Explicit expressions for the fields $A(t)$ and $F(t)$ used in our numerical examples are given in Sec. VI.]

To describe HHG and ATI in a short laser pulse of duration τ, we consider first the interaction of an atomic electron with an infinite train of short pulses separated in time by a period $\mathcal{T}$ (cf. Fig. 1). Each pulse of this train is the same as for an actual short laser pulse of duration τ described by Eqs. (1) and (2), while $\mathcal{T} > \tau$. The dipole interaction of such a pulse train (PT) with an atomic electron is given by

$$V_\tau(\mathbf{r}, t) = \sum_{n=-\infty}^{\infty} V(\mathbf{r}, t + n\mathcal{T}) = -\mathbf{d}\cdot\mathbf{F}_\tau(t), \tag{3}$$

where

$$\mathbf{F}_\tau(t) = -\frac{1}{c}\frac{\partial \mathbf{A}_\tau(t)}{\partial t} = \sum_{n=-\infty}^{\infty} \mathbf{F}(t + n\mathcal{T}),$$

$$\mathbf{A}_\tau(t) = \mathbf{e}_z A_\tau(t) = \sum_{n=-\infty}^{\infty} \mathbf{A}(t + n\mathcal{T}). \tag{4}$$

Owing to the periodicity of $V_\tau(\mathbf{r}, t)$ (with period $\mathcal{T}$), we can employ the QQES (or complex quasienergy) approach (cf., e.g., Ref. [44]) for an *ab initio* treatment of nonlinear interactions of the PT with an atomic system. From the QQES expressions for the HHG and ATI amplitudes and rates for the PT, the results for a *single* short pulse follow by taking the limit $\mathcal{T} \to \infty$ for fixed τ. Since the QQES approach has mainly been used previously for monochromatic or two-color fields $\mathbf{F}(t)$, in the next subsection we present the QQES results for ATI and HHG amplitudes and rates for the general case of a periodic field $\mathbf{F}(t)$, i.e., $\mathbf{F}(t) = \mathbf{F}_\tau(t)$, as in Eq. (3).

B. Basic QQES results for a periodic field

In the QQES approach, after adiabatic turn on of the interaction (3), the wave function of a bound electron with energy E_0 evolves to the wave function,

$$\Psi_\epsilon(\mathbf{r}, t) = e^{-i\epsilon t/\hbar}\Phi_\epsilon(\mathbf{r}, t), \quad \Phi_\epsilon(t) = \Phi_\epsilon(t + \mathcal{T}), \tag{5}$$

with the complex quasienergy $\epsilon = \mathrm{Re}\,\epsilon - (i\hbar/2)\Gamma$, where Γ is the total ionization rate of the initial bound state due to the field $\mathbf{F}_\tau(t)$, while $\mathrm{Re}\,\epsilon \to E_0$ as $\mathbf{F}_\tau(t) \to 0$. Since we are describing the ionization of a bound state, the periodic in time QQES wave function $\Phi_\epsilon(\mathbf{r}, t)$ satisfies the following complex boundary condition in open n-photon ionization channels for $r \to \infty$:

$$\Phi_\epsilon(\mathbf{r}, t) \sim \sum_{n \geq n_0} \mathcal{A}_n(\mathbf{p}_n)\frac{e^{ik_n R - in\omega_\tau t}}{R}, \tag{6}$$

$$k_n = \sqrt{2m(\epsilon + n\hbar\omega_\tau - u_p)}\Big/\hbar, \tag{7}$$

$$u_p = \frac{e^2}{2mc^2\mathcal{T}}\int_{-\mathcal{T}/2}^{\mathcal{T}/2} \mathbf{A}_\tau^2(t)dt = \frac{e^2}{2mc^2\mathcal{T}}\int_{-\mathcal{T}/2}^{\mathcal{T}/2} \mathbf{A}^2(t)dt, \tag{8}$$

$$\mathbf{R} \equiv \mathbf{R}(\mathbf{r}, t) = \mathbf{r} - \frac{|e|}{mc}\int^t \mathbf{A}_\tau(t')dt', \tag{9}$$

where $\omega_\tau = 2\pi/\mathcal{T}$, and $n_0 = [(u_p - \mathrm{Re}\,\epsilon)/(\hbar\omega_\tau)]$, where $[x]$ denotes the integer part of x. $\mathcal{A}_n(\mathbf{p}_n)$ is the amplitude for ATI with absorption of n photons of energy $\hbar\omega_\tau$ and photoelectron momentum $\mathbf{p}_n = p_n\hat{\mathbf{r}}$, where $\hat{\mathbf{r}} \equiv \mathbf{r}/r$ and

$$p_n = \sqrt{2m(\mathrm{Re}\,\epsilon + n\hbar\omega_\tau - u_p)}. \tag{10}$$

The differential n-photon ATI rate, $d\Gamma(\mathbf{p}_n)/d\Omega_{\mathbf{p}_n} \equiv \Gamma(\mathbf{p}_n)$, is given by

$$\Gamma(\mathbf{p}_n) = \frac{\hbar}{m}\left|\sqrt{k_n}\mathcal{A}_n(\mathbf{p}_n)\right|^2. \tag{11}$$

Note that Eqs. (6)–(11) reduce in the case of a monochromatic field to the QQES results obtained in Refs. [45, 46]. Thus, as in the case of a monochromatic field, the ATI amplitude for the PT field $\mathbf{F}_\tau(t)$ requires for its definition only the asymptotic form of the QQES wave function.

An atom interacting with a non-monochromatic PT field $\mathbf{F}_\tau(t)$ emits harmonics with frequencies $\Omega = N\omega_\tau$, where N is an integer that may be both *odd* and *even*. Similarly to the QQES result for a monochromatic field [40], the harmonic generation amplitude, $\mathcal{A}_\Omega$, can be expressed in terms of the complex quasienergy ε of an atom in two fields, the strong field $\mathbf{F}_\tau(t)$ and a weak (infinitesimal) harmonic field $\mathbf{F}_h(t) = \mathbf{e}_z F_h\cos(\Omega t + \phi_h)$:

$$\mathcal{A}_\Omega = -4\frac{\partial\varepsilon}{\partial\tilde{F}_h}\bigg|_{F_h=0}, \quad \tilde{F}_h = F_h e^{i\phi_h}. \tag{12}$$

¿From the definition (12) for the HHG amplitude, the HHG rate for a harmonic with frequency Ω is [40]:

$$\mathcal{R}_\Omega = \frac{\Omega^3|\mathcal{A}_\Omega|^2}{8\pi\hbar c^3}. \tag{13}$$

Note that, as shown in Ref. [40], the harmonic amplitude $\mathcal{A}_\Omega$ in Eq. (12) equals the Fourier-component $\tilde{\mathcal{D}}_\Omega$ of the dual dipole moment [47, 48], $\tilde{\boldsymbol{\mathcal{D}}}(t) = \mathbf{e}_z\tilde{\mathcal{D}}(t)$, where

$$\tilde{\mathcal{D}}_\Omega = \frac{2}{\mathcal{T}}\int_{-\mathcal{T}/2}^{\mathcal{T}/2}\tilde{\mathcal{D}}(t)e^{i\Omega t}dt, \tag{14}$$

C. General definitions of ATI and HHG probabilities for the case of a short pulse

In the case of a short laser pulse, both the photoelectron and the generated radiation spectra are continuous. Thus the concept of a rate cannot be used to describe ATI and HHG spectra. Instead some continuous functions of electron energy E_p and frequency Ω (or photon energy $E_\Omega = \hbar\Omega$) should be introduced in this case.

We start with ATI, in which case the doubly differential probability to detect the photoelectron in the energy interval $(E_p, E_p + dE_p)$ and in the solid angle $d\Omega_{\mathbf{p}}$,

$$\mathcal{P}(\mathbf{p}) \equiv \frac{d^2P}{dE_p d\Omega_{\mathbf{p}}}, \tag{15}$$

is the proper quantity for describing ATI by a single short pulse. To find an expression for $\mathcal{P}(\mathbf{p})$, we consider first the total ionization probability $\Gamma_{\rm tot}$ for a period $\mathcal{T}$ of the PT field $\mathbf{F}_\tau(t)$:

$$\Gamma_{\rm tot} = \mathcal{T}\sum_{n\geq n_0}\int d\Omega_{\mathbf{p}_n}\Gamma(\mathbf{p}_n), \tag{16}$$

where we have approximated ϵ by E_0 in Eq. (7), so that $n_0 = [(u_p - E_0)/(\hbar\omega_\tau)]$, $p_n = \sqrt{2m(E_0 + n\hbar\omega_\tau - u_p)}$, and $k_n = p_n/\hbar$. In the limit $\omega_\tau \to 0$, the sum over n in Eq. (16) can be replaced by an integral over the electron's momentum p [or energy $E_p = p^2/(2m)$], substituting

$$p_n = \sqrt{2m(n\hbar\omega_\tau + E_0 - u_p)} \to p, \tag{17}$$

$$\sum_{n>n_0} \to \frac{1}{m\hbar\omega_\tau}\int p\,dp = \frac{1}{\hbar\omega_\tau}\int dE_p. \tag{18}$$

The result is:

$$\Gamma_{\rm tot} = \frac{2\pi}{\hbar\omega_\tau^2}\int\int \Gamma(\mathbf{p})dE_p d\Omega_{\mathbf{p}}, \tag{19}$$

where

$$\Gamma(\mathbf{p}) = \frac{p}{m}|\mathcal{A}(\mathbf{p})|^2, \quad \mathcal{A}(\mathbf{p}) \equiv \mathcal{A}_n(\mathbf{p}_n)\Big|_{\mathbf{p}_n=\mathbf{p}}. \tag{20}$$

Thus the desired short pulse probability $\mathcal{P}(\mathbf{p})$ is given by

$$\mathcal{P}(\mathbf{p}) = \frac{2\pi p}{m\hbar}\lim_{\omega_\tau\to 0}\frac{|\mathcal{A}(\mathbf{p})|^2}{\omega_\tau^2}. \tag{21}$$

To describe harmonic generation by an atom in a short laser pulse, we use the spectral density of radiation, $\rho(E_\Omega)$. Consider first the total energy radiated during a period $\mathcal{T}$ of the PT $\mathbf{F}_\tau(t)$:

$$\mathcal{E}_{\rm tot} = \mathcal{T}\sum_N \hbar\Omega\mathcal{R}_\Omega. \tag{22}$$

As for the case of ATI, in the limit $\mathcal{T}\to\infty$, the sum in Eq. (22) can be replaced by the integral:

$$\mathcal{E}_{\rm tot} = \lim_{\omega_\tau\to 0}\frac{2\pi}{\omega_\tau^2}\int dE_\Omega\Omega\mathcal{R}_\Omega \equiv \int dE_\Omega\rho(E_\Omega),$$

where the spectral density $\rho(E_\Omega)$ is:

$$\rho(E_\Omega) = 2\pi\Omega\lim_{\omega_\tau\to 0}\frac{\mathcal{R}_\Omega}{\omega_\tau^2}. \tag{23}$$

We emphasize that the limit in Eq. (23) is taken at fixed Ω. Generalization of the concept of a dual dipole moment to the case of a short laser pulse is obtained by substituting Eq. (13) for $\mathcal{R}_\Omega$ into Eq. (23) (using $\mathcal{A}_\Omega = \tilde{\mathcal{D}}_\Omega$):

$$\rho(E_\Omega) = \frac{\Omega^4}{4\hbar c^3}|\tilde{\mathcal{D}}(\Omega)|^2. \tag{24}$$

The Fourier-transform, $\tilde{\mathcal{D}}(\Omega)$, of the dual dipole moment for a single short pulse is defined by the formal limit:

$$\tilde{\mathcal{D}}(\Omega) = \lim_{\omega_\tau\to 0}\tilde{\mathcal{D}}_\Omega/\omega_\tau, \tag{25}$$

where $\tilde{\mathcal{D}}_\Omega$ [cf. Eq. (14)] is the Fourier-component of the dual dipole moment for a periodic field.

The formal definitions in Eqs. (21) and (23) for $\mathcal{P}(\mathbf{p})$ and $\rho(E_\Omega)$ in terms of ATI and HHG rates for a periodic field are quite general and are valid for any atomic system. However, in practice appropriate expressions for $\mathcal{A}_n(\mathbf{p}_n)$ and $\tilde{\mathcal{D}}_\Omega$ are necessary in order that the limits in Eqs. (21) and (25) can be calculated. Such expressions are most easily obtained only for model systems, such as the one used in the TDER theory [36, 37] to analyze strong field processes in a monochromatic field. In Sec. III we describe briefly basic results of this model for the case of a periodic field, which will then be used to specify the spectral density (23) for a short pulse in the framework of TDER theory. (The TDER results for ATI by a short laser pulse will be published elsewhere.)

III. TDER RESULTS FOR THE COMPLEX QUASIENERGY IN A PERIODIC FIELD

Within TDER theory [36, 37] calculations of the complex quasienergy ε in Eq. (12) simplify so that most can be carried out analytically. This theory treats the electron in a short-range potential $U(r)$ (of radius r_c) that supports only a single bound state $\psi_{\kappa lm}(\mathbf{r})$ with energy $E_0 = (\hbar\kappa)^2/(2m)$, angular momentum l, and the following asymptotic behavior at large distances:

$$\psi_{\kappa lm}(\mathbf{r})|_{\kappa r\gg 1} = C_{\kappa l}\sqrt{\kappa}r^{-1}e^{-\kappa r}Y_{lm}(\hat{\mathbf{r}}), \tag{26}$$

where $C_{\kappa l}$ is a (dimensionless) asymptotic coefficient. In the TDER model the interaction of the active electron with the potential $U(r)$ is described by the l-wave scattering phase shift $\delta_l(k)$ ($k=\sqrt{2mE/\hbar^2}$). This phase is parameterized within effective range theory [49] in terms of the scattering length (a_l) and the effective range (r_l), which are the parameters of the problem.

The solution of the QQES problem within the TDER model simplifies significantly owing to the boundary condition for the QQES wave function $\Phi_\varepsilon(\mathbf{r},t)$ in this model at small distances, $r \lesssim r_c$ (cf. Refs. [36, 37] for details):

$$\int \Phi_\varepsilon(\mathbf{r},t)Y^*_{lm}(\hat{\mathbf{r}})d\Omega \sim \left[\frac{1}{r^{l+1}}+\cdots+B_l(\varepsilon)(r^l+\cdots)\right]g(t) + i\frac{2l+1}{[(2l+1)!!]^2}\frac{mr_l}{\hbar}(r^l+\cdots)\frac{d}{dt}g(t), \quad (27)$$

where ε is the complex quasienergy in the combined field $\boldsymbol{\mathcal{F}}(t)$, which is required for calculation of the HHG amplitude according to Eq. (12):

$$\boldsymbol{\mathcal{F}}(t)=\mathbf{e}_z\mathcal{F}(t)=\mathbf{F}_\tau(t)+\mathbf{F}_h(t). \quad (28)$$

In Eq. (27), $g(t)$ is a periodic function with period $\mathcal{T}$, and the parametrization of the coefficient $B_l(\varepsilon)$ is very similar to that for the scattering phase $\delta_l(k)$ [49]:

$$(2l-1)!!(2l+1)!!B_l(\varepsilon)=k^{2l+1}\cot\delta_l(k) = -\frac{1}{a_l}+\frac{1}{2}r_lk^2, \quad k=\sqrt{2m\varepsilon/\hbar^2}.$$

Within the TDER theory, the four-dimensional (in $\mathbf{r}$ and t) TDSE for ε and $\Phi_\varepsilon(\mathbf{r},t)$ reduces to a homogeneous one-dimensional integro-differential equation (a key advantage), representing an eigenvalue problem for ε and $g(t)$. For a bound s-state, this equation is (cf. the similar results for a monochromatic field in [36, 37]):

$$g(t)-\frac{\kappa r_0}{2|E_0|}\left(\Delta\varepsilon g(t)+i\hbar\frac{dg(t)}{dt}\right) = \frac{2\pi\hbar^2}{\kappa m}\int_0^\infty d\tau\left[G(t,t-\tau)g(t-\tau)e^{i\varepsilon\tau}- -G^{(0)}(t,t-\tau)g(t)\right]. \quad (29)$$

Here $\Delta\varepsilon=\varepsilon-E_0$, $G^{(0)}(t,t-\tau)\equiv G^{(0)}(\mathbf{r}=0,t;\mathbf{r}'=0,t-\tau)$ is the ordinary retarded Green function for a free electron, and $G(t,t-\tau)\equiv G(\mathbf{r}=0,t;\mathbf{r}'=0,t-\tau)$ is that for an electron in the field $\boldsymbol{\mathcal{F}}(t)$. Equation (29) and the equivalent infinite system of homogeneous linear equations for ε and the Fourier-coefficients of the function $g(t)$ are convenient for numerical analyses. However, for analytical analyses it is more convenient to represent Eq. (29) in terms of the quasienergy representations, $\mathcal{G}^{(0)}_\varepsilon(t,t-\tau)$ and $\mathcal{G}_\varepsilon(t,t-\tau)$, of the Green functions $G^{(0)}(t,t-\tau)$ and $G(t,t-\tau)$. [An explicit form of $\mathcal{G}_\varepsilon(\mathbf{r},t;\mathbf{r}',t')$ for a monochromatic field can be found in Ref. [50].] Using the relation between $G(\mathbf{r},t;\mathbf{r}',t')$ and $\mathcal{G}_\varepsilon(\mathbf{r},t;\mathbf{r}',t')$ [50] (cf. also Appendix B in Ref. [41]), the integral term in Eq. (29) can be represented as:

$$\int_0^\infty\left[G(t,t-\tau)g(t-\tau)e^{\frac{i}{\hbar}\varepsilon\tau}-G_0(t,t-\tau)g(t)\right]d\tau = \frac{1}{\mathcal{T}}\int_{-\mathcal{T}/2}^{\mathcal{T}/2}\tilde{\mathcal{G}}_\varepsilon(t,t')g(t')dt', \quad (30)$$

where

$$\tilde{\mathcal{G}}_\varepsilon(t,t')\equiv\mathcal{G}_\varepsilon(t,t')-\mathcal{G}^{(0)}_\varepsilon(t,t') = -\frac{m}{2\pi\hbar^2}\exp\left(-\frac{i}{\hbar}\int_{t'}^t\left[\frac{e^2\mathcal{A}^2(t'')}{2mc^2}-\tilde{u}_p\right]dt''\right) \times\sum_n\frac{e^{-in\omega_\tau(t-t')}\left(e^{i\tilde{k}_n|\mathcal{R}(t,t')|}-1\right)}{|\mathcal{R}(t,t')|}, \quad (31)$$

$$\mathcal{R}(t,t')=\frac{|e|}{mc}\int_{t'}^t\mathcal{A}(t'')dt'', \quad (32)$$

$$\mathcal{A}(t)=A_\tau(t)-\frac{cF_h}{\Omega}\sin(\Omega t+\phi_h), \quad (33)$$

$$\tilde{u}_p=\frac{e^2}{2mc^2\mathcal{T}}\int_{-\mathcal{T}/2}^{\mathcal{T}/2}\mathcal{A}^2(t)dt, \quad (34)$$

$$\frac{\hbar^2\tilde{k}_n^2}{2m}=n\hbar\omega_\tau+\varepsilon-\tilde{u}_p, \quad (35)$$

and $\boldsymbol{\mathcal{A}}(t)=\mathbf{e}_z\mathcal{A}(t)$ is the vector-potential of the field $\boldsymbol{\mathcal{F}}(t)$. The result is the following alternative form of the basic TDER equation (29) for a periodic field:

$$g(t)-\frac{\kappa r_0}{2|E_0|}\left(\Delta\varepsilon g(t)+i\hbar\frac{dg(t)}{dt}\right) = \frac{2\pi\hbar^2}{m\kappa\mathcal{T}}\int_{-\mathcal{T}/2}^{\mathcal{T}/2}\tilde{\mathcal{G}}_\varepsilon(t,t')g(t')dt'. \quad (36)$$

IV. QUASICLASSICAL RESULTS FOR THE HHG AMPLITUDE AND SPECTRAL DENSITY $\rho(E_\Omega)$ IN TDER THEORY

We consider harmonic generation by a short pulse whose vector potential, $A(t)$, and electric field, $F(t)$, are slowly varying on the atomic time scale of order $T_0=\hbar/|E_0|$. For a short pulse with carrier frequency ω, this is equivalent to

$$\hbar\omega\ll|E_0|. \quad (37)$$

Moreover, we assume that

$$\max\{F(t)\}\ll F_0, \qquad F_0=\sqrt{8m|E_0|^3}/(|e|\hbar), \quad (38)$$

where $\max\{F(t)\}$ is the maximum value of $F(t)$ in the interval $(0,\tau)$. When the conditions (37) and (38) are fulfilled, the TDER result for $\rho(E_\Omega)$ can be obtained in analytic form in the quasiclassical approximation. In order to carry out the limiting procedure in Eq. (25), we obtain first the quasiclassical result for the HHG amplitude $\tilde{\mathcal{D}}_\Omega$ for small, but finite ω_τ, e.g., $\omega_\tau\ll\omega$.

A. Analytic results for a periodic field

Since for a slowly-varying short pulse the function $g(t)$ in Eq. (36) also varies slowly with t, we can set $g(t) =$ const and then average Eq. (36) in t over the period $\mathcal{T}$. (This procedure is similar to the adiabatic approximation used for the case of a monochromatic field [51] and its accuracy for describing HHG for this case is discussed in Ref. [41]). Thus, Eq. (36) reduces to a transcendental equation for the complex quasienergy ε:

$$1 - \frac{\kappa r_0}{2|E_0|}(\varepsilon - E_0) = \mathcal{I}(\varepsilon, F_h), \tag{39}$$

where

$$\mathcal{I}(\varepsilon, F_h) = \frac{2\pi\hbar^2}{m\kappa\mathcal{T}^2}\iint_{-\mathcal{T}/2}^{\mathcal{T}/2} \tilde{\mathcal{G}}_\varepsilon(t,t')dtdt'. \tag{40}$$

[Note that Eq. (39) at $F_h = 0$ gives the transcendental equation for the quasienergy ϵ in the PT field $\mathbf{F}_\tau(t)$.]

Approximating $\varepsilon = \epsilon + \Delta\epsilon$ (where $\Delta\epsilon \propto F_h$) and expanding the right side of Eq. (39) to first order in both F_h and $\Delta\epsilon$, we obtain an expression for the linear (in F_h) correction $\Delta\epsilon$ to the complex quasienergy ϵ in the PT field $\mathbf{F}_\tau(t)$ induced by a weak harmonic field $\mathbf{F}_h(t)$:

$$\Delta\epsilon = -F_h \frac{\mathcal{I}'_{F_h}(\epsilon, 0)}{\kappa r_0/(2|E_0|) + \mathcal{I}'_\varepsilon(\epsilon, 0)}, \tag{41}$$

where $\mathcal{I}'_x \equiv \partial\mathcal{I}/\partial x$. In the quasiclassical approximation, the quasienergy ϵ in Eq. (41) can be approximated by E_0. Moreover, the denominator in Eq. (41) is connected to the normalization factor for the QQES wave function [36, 37] and may be approximated by its unperturbed value:

$$\kappa r_0/(2|E_0|) + \mathcal{I}'_\epsilon(\epsilon, 0) \approx -(|E_0|C_{\kappa 0}^2)^{-1},$$

where the asymptotic coefficient $C_{\kappa 0}$ is defined by Eq. (26). Thus the result (41) for $\Delta\epsilon$ reduces to:

$$\Delta\epsilon = F_h C_{\kappa 0}^2 \mathcal{I}'_{F_h}(E_0, 0)|E_0|. \tag{42}$$

As shown in Appendix A, the derivative $\mathcal{I}'_{F_h}$ can be parameterized in terms of Fourier-components $\tilde{\mathcal{D}}_{\pm\Omega}$ of the dual dipole moment [cf. Eq. (14)]:

$$4C_{\kappa 0}^2|E_0|\mathcal{I}'_{F_h}(E_0, 0) = \tilde{\mathcal{D}}_\Omega e^{i\phi_h} + \tilde{\mathcal{D}}_{-\Omega}e^{-i\phi_h}, \tag{43}$$

where the HHG amplitude $\tilde{\mathcal{D}}_\Omega$ can be expressed as:

$$\tilde{\mathcal{D}}_\Omega = i\hbar^3\sqrt{\frac{2\pi\kappa|e|}{m^3}}\frac{1}{\mathcal{T}^2}\sum_{n>n_0}^{\infty}\sum_\nu\sum_{\sigma=\pm1} d_n^{\sigma\nu}, \tag{44}$$

$$d_n^{\sigma\nu} = \frac{C_{\kappa 0}^2}{\sqrt{\sigma F(t_\nu^\sigma)}} \times \int_{-\mathcal{T}/2}^{\mathcal{T}/2} \frac{e^{-iS(t,t_\nu^\sigma;p_n)/\hbar + i\Omega t}P_\sigma(t;p_n)}{R(t,t_\nu^\sigma)\left[\frac{[P_\sigma(t;p_n)]^2}{2m} - E_0\right]^2}dt, \tag{45}$$

where

$$P_\sigma(t;p) = p + \sigma\frac{|e|}{c}A(t), \tag{46}$$

$$p_n = \sqrt{2m(n\hbar\omega_\tau + E_0 - u_p)},$$

$$S(t,t_1;p) = \int_{t_1}^{t}\left(\frac{[P_\sigma(t';p)]^2}{2m} - E_0\right)dt', \tag{47}$$

$$R(t,t_1) = \frac{|e|}{mc}\int_{t_1}^{t} A(t')dt'. \tag{48}$$

The labeled times t_ν^σ $[= t_\nu^\sigma(p_n)]$ in Eq. (45) are roots of the saddle point equation,

$$P_\sigma(t_\nu^\sigma; p_n) = -i\hbar\kappa, \tag{49}$$

having positive imaginary part, $\mathrm{Im}\, t_\nu^\sigma$.

As in the monochromatic field case [52], Eqs. (44), (45) for the HHG amplitude of a PT field $\mathbf{F}_\tau(t)$ have a clear physical interpretation. They express the HHG amplitude as a coherent sum of partial amplitudes corresponding to the generation of harmonics by an electron created in the continuum by n-photon ATI. For a given n, these amplitudes are determined by the saddle points t_ν^σ of the classical action $S(t,t_1;p_n)$ [cf. Eq. (49)], which may be interpreted as complex "ionization times." Finally, $\sigma = \pm1$ distinguishes electrons escaping in opposite directions along the polarization vector $\mathbf{e}_z$. The number of saddle points t_ν^σ contributing to the sum over ν in Eq. (44) depends on the shape of the vector potential $A(t)$. For a monochromatic field of frequency ω_τ, only two saddle points (with $\sigma = \pm1$) contribute, in which case our results (44), (45) coincide with those of Ref. [52] as well as with those obtained within the quasiclassical approximation for the TDER model [41].

B. Analytic results for a short pulse

To apply the quantum results (44), (45) for the HHG amplitude $\tilde{\mathcal{D}}_\Omega$, obtained for the case of a finite ω_τ, to the case of a single short pulse (i.e., in the limit $\omega_\tau \to 0$), we use the definition of the Fourier-transform $\tilde{\mathcal{D}}(\Omega)$ in Eq. (25). Replacing the sum over n in Eq. (44) by an integral over the electron's momentum p according to Eqs. (17) and (18), the right side of Eq. (44) becomes proportional to $1/\mathcal{T}$ $[= \omega_\tau/(2\pi)]$. The limit $\omega_\tau \to 0$ in Eq. (25) is thus finite, giving the result

$$\tilde{\mathcal{D}}(\Omega) = \frac{1}{\pi}\int_{-\infty}^{\infty}\tilde{\mathcal{D}}(t)e^{i\Omega t}dt, \tag{50}$$

where

$$\tilde{\mathcal{D}}(t) = i\sqrt{\frac{|e|}{2\pi(m\kappa)^3}}\sum_{\sigma=\pm1}\int_0^\infty dp\sum_\nu d_\nu^\sigma(p,t),$$

$$d_\nu^\sigma(p,t) = \frac{|E_0|C_{\kappa 0}^2 e^{-iS(t,t_\nu^\sigma;p)/\hbar}P_\sigma(t;p)p}{\sqrt{\sigma F(t_\nu^\sigma)}R(t,t_\nu^\sigma)\left[\frac{[P_\sigma(t;p)]^2}{2m} - E_0\right]^2}. \tag{51}$$

Approximate evaluations of the integrals in Eqs. (50) and (51) (derived in Appendix B) lead to further simplifications of the HHG amplitude $\tilde{\mathcal{D}}(\Omega)$ for a single short pulse. For a short pulse with given carrier frequency, ω, and carrier-envelope phase (CEP), ϕ, we parametrize the vector potential $A(t)$ in Eq. (1) as follows:

$$A(t) = f(t)\sin(\omega t + \phi), \tag{52}$$

where the pulse envelope, $f(t)$, has its maximum at $t = 0$.

The results in Appendix B, derived for a vector potential $A(t)$ of arbitrary form, show that when $A(t)$ has the form in Eq. (52), then the generation amplitude has the form presented in Ref. [22], i.e., a coherent sum of partial amplitudes A_j describing the generation of radiation with frequency Ω by electrons ionized at each (jth) optical half-cycle of the pulse described by (52):

$$\tilde{\mathcal{D}}(\Omega) = \sqrt{-i}\frac{|e|a_0}{\omega}\sum_j (-1)^j A_j e^{i\varphi_j}, \tag{53}$$

$$A_j = \chi_\tau^{(j)}\chi_w^{(j)}\chi_\sigma(E), \tag{54}$$

$$\hbar\varphi_j = E_\Omega t_r^{(j)} - \int_{t_i^{(j)}}^{t_r^{(j)}} \left[\mathcal{E}_{\max}^{\rm cl}(t_i^{(j)}, t) - E_0\right] dt, \tag{55}$$

where $E_\Omega = \hbar\Omega$, $E = E_\Omega - |E_0|$, and the index j enumerates the ionization ($t_i^{(j)}$) and recombination ($t_r^{(j)}$) times for the jth *half-cycle* [where $t_r^{(j)}$ lies in the $(j+1)$th half-cycle]. These times satisfy equations for the extreme closed classical trajectory (starting and ending at times $t_i^{(j)}$ and $t_r^{(j)}$) along which an electron having zero initial velocity gains the maximum classical energy, $\mathcal{E}_{\max}^{\rm cl}(t_i^{(j)}, t_r^{(j)})$:

$$A(t_i^{(j)}) - \frac{1}{t_r^{(j)} - t_i^{(j)}}\int_{t_i^{(j)}}^{t_r^{(j)}} A(t)dt = 0, \tag{56}$$

$$\frac{1}{c}\frac{A(t_r^{(j)}) - A(t_i^{(j)})}{t_r^{(j)} - t_i^{(j)}} + F(t_r^{(j)}) = 0. \tag{57}$$

Each dimensionless partial amplitude A_j in Eq. (54) has three factors, in accord with the three-step scenario for HHG: ionization of the active electron in an atom by laser-induced tunneling, propagation along a closed trajectory driven by the laser field, and, finally, recombination to the initial bound state of the parent atom accompanied by emission of a harmonic photon $\hbar\Omega$ [10, 11].

The tunneling factor (χ_τ) in Eq. (54) has the form:

$$\chi_\tau^{(j)} = \frac{4C_{k0}\tilde{\gamma}_j}{(\kappa a_0)^2}\sqrt{\frac{\tilde{F}_j}{F_0}}e^{-F_0/(3\tilde{F}_j)}, \quad \tilde{\gamma}_j = \frac{\sqrt{2m|E_0|}\omega}{|e|\tilde{F}_j} \tag{58}$$

where $\tilde{F}_j \equiv \tilde{F}(t_i^{(j)})$ [cf. Eq. (B17)], $F_0 = (\kappa a_0)^3 F_{\rm at}$, $F_{\rm at} = |e|/a_0^2$, $a_0 = \hbar^2/(me^2)$ is the Bohr radius, and $\tilde{\gamma}_j$ is an effective value of the Keldysh parameter γ [53] for the jth half-cycle. We emphasize that the true physical meaning of the factor $\chi_\tau^{(j)}$ is that it is the detachment amplitude for low-energy [$E = p^2/(2m) \to 0$] electrons ejected by a laser pulse along its polarization axis. In the tunneling regime, the dominant term in an expansion of the short-pulse detachment amplitude, $\mathcal{A}(\mathbf{p}, F)$, in the Keldysh parameter has a form similar to that for a monochromatic field with amplitude F [54] (cf. Ref. [55]):

$$\mathcal{A}(\mathbf{p} = 0, F) = \frac{C_{\kappa 0}\sqrt{\kappa}\gamma}{2\pi}\sqrt{\frac{F}{F_0}}e^{-F_0/(3F)}. \tag{59}$$

Comparing Eqs. (58) and (59), $\chi_\tau^{(j)}$ can be presented in terms of the detachment amplitude:

$$\chi_\tau^{(j)} = 8\pi\mathcal{A}(\mathbf{p} = 0, \tilde{F}_j)/(\kappa^{5/2}a_0^2). \tag{60}$$

The factor $\chi_w^{(j)}$ in Eq. (54) describes propagation of an electron (tunnel-ionized in the jth half-cycle) in the laser-dressed continuum. It involves an Airy function $\mathrm{Ai}(\xi_j)$:

$$\chi_w^{(j)} = \frac{\mathrm{Ai}(\xi_j)}{\zeta_j^{1/3}(\omega_{\rm at}\Delta t_j)^{3/2}}, \tag{61}$$

where $\Delta t_j = t_r^{(j)} - t_i^{(j)}$,

$$\zeta_j = -\frac{I(t_r^{(j)})}{2I_{\rm at}}\left(1 - \frac{F(t_r^{(j)})}{F(t_i^{(j)})} + \frac{\dot{F}(t_r^{(j)})}{F(t_r^{(j)})}\Delta t_j\right), \tag{62}$$

$$\xi_j = \frac{E - E_{\max}^{(j)}}{\zeta_j^{1/3}E_{\rm at}}, \tag{63}$$

$$E_{\max}^{(j)} = \mathcal{E}_{\max}^{\rm cl}(t_i^{(j)}, t_r^{(j)}) - \frac{F(t_r^{(j)})}{F(t_i^{(j)})}|E_0|, \tag{64}$$

$$\mathcal{E}_{\max}^{\rm cl}(t_i^{(j)}, t_r^{(j)}) = \frac{e^2}{2mc^2}\left(A(t_r^{(j)}) - A(t_i^{(j)})\right)^2, \tag{65}$$

and $\omega_{\rm at} = 2.6\times10^{17}$ s^{-1}, $E_{\rm at} = 27.21$ eV, $I_{\rm at} = 3.51\times10^{16}$ W/cm^2.

The last factor, $\chi_\sigma(E)$, in Eq. (54) describes the recombination step of the three-step scenario:

$$\chi_\sigma(E) = C_{\kappa 0}\frac{q}{(q^2+1)^2}, \tag{66}$$

where $q = \sqrt{E/|E_0|} = p/(\hbar\kappa)$.

Substituting the amplitude (53) into Eq. (24), the spectral density $\rho(E_\Omega)$ acquires the factorized form [26–28]:

$$\rho(E_\Omega) = w(E, F)\sigma^{(r)}(E). \tag{67}$$

Here $\sigma^{(r)}(E)$ is the TDER result for the differential PRCS of an electron with momentum $\mathbf{p}$ ($p = \sqrt{2mE}$) parallel to the polarization direction $\mathbf{e}_z$ of the harmonic (recombination) photon of energy E_Ω (cf. Ref. [42]):

$$\sigma^{(r)}(E) = \alpha^3\chi_\sigma^2(E)\frac{(q^2+1)^3}{q}a_0^2, \quad \alpha = e^2/(\hbar c). \tag{68}$$

The term $w(E, F)$ in Eq. (67) is the EWP, which can be presented as follows:

$$w(E, F) = \sum_{j,k} s_{jk}\sqrt{w_j w_k}\cos(\varphi_j - \varphi_k), \tag{69}$$

where $s_{jk} \equiv (-1)^{j-k}\mathrm{sign}(\chi_w^{(j)}\chi_w^{(k)})$. As for the case of a monochromatic field [25], the partial EWP w_j for the jth half-cycle can be presented as a product of tunneling ($\mathcal{I}_j$) and propagation ($\mathcal{W}_j$) factors:

$$w_j = \frac{\pi\Omega}{2\omega^2}\mathcal{I}_j\mathcal{W}_j, \tag{70}$$

$$\mathcal{I}_j = \frac{1}{16\pi}(\chi_\tau^{(j)})^2(\kappa a_0)^5 = \frac{4\tilde{\gamma}_j^2\Gamma_{\rm st}(\tilde{F}_j)}{\pi\kappa v_{\rm at}}, \tag{71}$$

$$\mathcal{W}_j = \frac{p}{ma_0^3}(\chi_w^{(j)})^2 = \frac{p}{m}\frac{\mathrm{Ai}^2(\xi_j)}{(v_{\rm at}\Delta t_j)^3\zeta_j^{2/3}}, \tag{72}$$

where $\Gamma_{\rm st}(\tilde{F}_j)$ is the decay rate for a weakly-bound s-state electron in a static electric field $\mathbf{F}$ [56]:

$$\Gamma_{\rm st}(F) = C_{\kappa 0}^2\frac{F}{2F_0}e^{-2F_0/(3\tilde{F})}\frac{|E_0|}{\hbar}. \tag{73}$$

As Eqs. (70) – (72) show, the magnitude of the j-th EWP w_j is governed by the DC ionization rate $\Gamma_{\rm st}(\tilde{F}_j)$, where $\tilde{F}_j$ is close to the maximum value of the field $F(t)$ during the jth half-cycle. Since the magnitude of $\Gamma_{\rm st}(\tilde{F}_j)$ decreases exponentially with decreasing $\tilde{F}_j$, only a few optical half-cycles near the peak intensity of a short pulse contribute significantly to the sum in Eq. (69). For each half-cycle, the propagation factor $\mathcal{W}_j$ describes plateau structures in the spectrum of harmonics generated by electrons created during this half-cycle. In particular, the position of the jth plateau cutoff, $E_{\rm cut}^{(j)}$, is given by an equation similar to that for a monochromatic field [42]:

$$E_{\rm cut}^{(j)} = |E_0| + \mathcal{E}_{\max}^{\rm cl}(t_i^{(j)}, t_r^{(j)}) - \frac{F(t_r^{(j)})}{F(t_i^{(j)})}|E_0| - 1.019\zeta_j^{1/3}E_{\rm at}. \tag{74}$$

V. GENERALIZATION TO THE ATOMIC CASE

The TDER results for $\rho(\Omega)$ presented in Sec. IV are valid for a weakly-bound electron in an s-state. However, we have confirmed that the derivations described in Appendix B can be generalized for the case of a weakly-bound state with nonzero angular momentum l in a way similar to that used to obtain our TDER HHG results for a bound p-state in a monochromatic field [41]. As in the latter case, since the centrifugal barrier suppresses the return of a continuum electron with $l > 0$ to the atomic core, the harmonic yield for substates with nonzero angular momentum projection m (in which case $l \geq |m|$) is suppressed by a factor $(|E_0|\Delta t_j/\hbar)^{2|m|} \sim (|E_0|/\hbar\omega)^{2|m|}$ compared to the case $m = 0$. Nevertheless, our analysis (not presented) shows that the spectral density $\rho(\Omega)$ for $m = 0$ has the factorized form (67) with the *same* partial propagation factors (72) as for $l = 0$. Thus $\mathcal{W}_j$ is essentially independent of the spatial symmetry of the bound state, while both $\mathcal{I}_j$ and $\sigma(E)$ are sensitive to l. Moreover, we note that the TDER PRCS (68) coincides with that in the Born approximation since, as a consequence of dipole selection rules, it is determined by the p-wave scattering phase, which is zero in the TDER model for a single bound s-state. However, our recent analysis in Ref. [57] for the TDER model with two (s and p) bound states shows that, indeed, the TDER HHG results involve the *exact* (non-Born) result for the PRCS $\sigma(E)$.

The analytic results (67) – (72) describing HHG by a short laser pulse thus involve only two constituents, $\mathcal{I}_j$ and $\sigma(E)$, that depend on the atomic model employed. Since both of these constituents have a transparent physical meaning, it is reasonable to expect that the generalization of the TDER results for $\rho(\Omega)$ to the case of neutral atoms (as well as their positive and negative ions) requires only the replacement of $\mathcal{I}_j$ and $\sigma(E)$ by their corresponding atomic counterparts. The result (71) for $\mathcal{I}_j$ should thus be replaced by:

$$\mathcal{I}_j = \frac{4\tilde{\gamma}_j^2\Gamma_{\rm st}(\tilde{F}_j)}{(2l+1)\pi\kappa v_{\rm at}}, \tag{75}$$

$$\Gamma_{\rm st}(\tilde{F}_j) = \frac{|E_0|}{\hbar}(2l+1)C_{\kappa l}^2\left(\frac{2F_{\rm at}}{\tilde{F}_j}\right)^{2\nu-1}e^{-2F_{\rm at}/(3\tilde{F}_j)},$$

where $\Gamma_{\rm st}(F)$ is the tunneling rate for a bound atomic electron [in the state $\psi_{\kappa lm}(\mathbf{r})$ with energy E_0, angular momentum l, and projection $m = 0$] in a static electric field $\mathbf{e}\tilde{F}_j$ [56], and $C_{\kappa l}$ is determined by the asymptotic form of $\psi_{\kappa lm}(\mathbf{r})$ [cf. Eq. (26)]:

$$\psi_{\kappa lm}(\mathbf{r})|_{\kappa r\gg 1} = C_{\kappa l}\sqrt{\kappa}r^{-1}(\kappa r)^\nu e^{-\kappa r}Y_{lm}(\hat{\mathbf{r}}), \tag{76}$$

where $\nu = Z/(\kappa a_0)$ and Z is the charge of the atomic core. Also, the TDER PRCS (68) should be replaced by the corresponding cross section $\sigma^{(r)}(E)$ for the specific atom considered. For the ground state H atom, $\sigma^{(r)}(E)$ is known analytically [58],

$$\sigma^{(r)}(E) = 32\pi\alpha^3\frac{e^{-4q^{-1}\mathrm{arctan(q)}}}{q^2(1+q^2)^2(1-e^{2\pi/q})}a_0^2, \quad q = \frac{pa_0}{\hbar}, \tag{77}$$

while for other atoms experimental or theoretical data for $\sigma^{(r)}(E)$ should be used.

We present the resulting generalized expression for the spectral density $\rho(E_\Omega)$ in a way that separates terms with $j = k$ and $j \neq k$ in the sum in Eq. (69):

$$\rho(E_\Omega) = w(E)\sigma^{(r)}(E), \tag{78}$$

where the EWP $w(E)$ is given by:

$$w(E) = w_{\rm dir} + w_{\rm int}. \tag{79}$$

The "direct" term, $w_{\rm dir}$, includes only terms with $j = k$ and is given by the sum of half-cycle EWPs $w_j(E)$:

$$w_{\rm dir} = \sum_j w_j(E), \tag{80}$$

$$w_j(E) = \frac{\pi\Omega}{2\omega^2}\mathcal{I}_j\mathcal{W}_j, \tag{81}$$

where $\mathcal{I}_j$ and $\mathcal{W}_j$ are given by Eqs. (75) and (72). The "interference" term, $w_{\rm int}$, originates from the interference between the half-cycle amplitudes $\mathcal{A}_j$ and $\mathcal{A}_k$ ($j \neq k$) and thus involves their phase difference:

$$w_{\rm int} = \sum_{j\neq k} s_{kj} \sqrt{w_j(E) w_k(E)}\, \cos(\varphi_j - \varphi_k), \qquad (82)$$

where the phase φ_j is given by Eq. (55).

VI. NUMERICAL RESULTS

A. Comparison with TDSE results

In order to check the accuracy of our analytical results, we present comparisons with results of direct numerical solutions of the three-dimensional (3D) TDSE. The TDSE was solved by two different methods, both of which used the dipole length gauge:
(i) In spherical coordinates using a spherical harmonic expansion of the wave function (cf. Refs. [59, 60]);
(ii) In cylindrical coordinates using a split-step method with a fast Fourier transform with respect to z and a discrete Fourier-Bessel transform with respect to ρ (cf. Refs. [31, 61, 62]).

In the first method, $f(t)$ in Eq. (52) has a $\sin^2$-shape:

$$f(t) = -\frac{cF}{\omega} \begin{cases} \sin^2(\frac{t\pi}{\tau}), & t \in [0,\tau] \\ 0, & \text{otherwise} \end{cases}, \qquad (83)$$

where F is the peak value of the electric field $F(t)$, $\tau = 2\pi N/\omega$, and N is the number of optical cycles in the laser pulse. In Fig. 2 we present numerical results for a peak intensity $I = cF^2/(8\pi) = 10^{14}\,\mathrm{W/cm^2}$ and a wavelength $\lambda = 3.1\,\mu$m ($\hbar\omega = 0.4\,$eV). For these parameters, the convergence of the numerical results is achieved by solving the TDSE within the sphere defined by $0 \le r \le 5000\,a_0$, with a uniform radial grid step $\Delta r = 0.042\,a_0$, a uniform temporal step $\Delta t = 0.022\,t_{\rm at}$ ($t_{\rm at} = \hbar/E_{\rm at} \approx 2.42\times10^{-17}\,$s), and including orbital angular momenta L up to $L_{\max} = 500$.

In the second method, a Gaussian-like parametrization of the laser pulse is used:

$$\mathbf{A}(t) = \frac{\partial \boldsymbol{\mathcal{A}}(t)}{\partial t}, \quad \mathbf{F}(t) = -\frac{1}{c}\frac{\partial^2 \boldsymbol{\mathcal{A}}(t)}{\partial t^2}, \qquad (84)$$

$$\boldsymbol{\mathcal{A}}(t) = \mathbf{e}_z \frac{c\tilde{F}}{\omega^2} \tilde{f}(t) \cos(\omega t + \phi),$$

$$\tilde{F} = F\left(1 + \frac{\ln 2}{(\pi N)^2}\right)^{-1},$$

$$\tilde{f}(t) = \exp\left[-2\ln(2)\frac{t^2}{\tau_g^2}\right],$$

where $\tau_g = 2\pi N/\omega$, and N is the number of optical cycles in the full width at half maximum (FWHM). (Note that the FWHM for a $\sin^2$-shaped pulse is about three times smaller than for a Gaussian pulse with the same N.) Numerical results are presented for $\lambda = 1.6\,\mu$m ($\hbar\omega = 0.775\,$eV) and $I = 2\times10^{14}\,\mathrm{W/cm^2}$. Calculations for this case (cf. Fig. 3) were performed within the cylinder bounded by $-z_{\max} \le z \le z_{\max}$, $0 \le \rho \le \rho_{\max}$, with $z_{\max} = 614\,a_0$, $\rho_{\max} = 59\,a_0$. To avoid reflection from the boundary of the cylinder, the imaginary potential method [63] was used to absorb the wave function at the boundary. A uniform grid was used for both the integrations over time (with grid step size $\Delta t = 0.025\,t_a$) and over z (with $\Delta z = 0.3\,a_0$), whereas the grid nodes in ρ were placed nonuniformly: the grid was more dense near $\rho = 0$, and the total number of nodes, N_ρ, was 420.

As shown in Figs. 2 and 3, the results of the analytic formula in Eq. (78) are in excellent agreement with the numerical TDSE results, reproducing even the most minor details of the HHG spectra at the high-energy end of the plateaus. Small deviations of the analytic results from the TDSE results shown in Fig. 3 at the lower energy end of the HHG spectrum originate from the depletion ($\sim 20\%$) of the ground state in an intense field, whereas this depletion is negligible ($< 2\%$) for the longer wavelength results shown in Fig. 2. It is well established by many theoretical and experimental groups that the shape of $\rho(E_\Omega)$ depends crucially on the CEP [12–16, 18–21] (see also reviews [2, 7–9]); i.e., for $\phi = 0$ [cf. Figs. 2(a)-(c) and 3(a)], two-plateau structures in HHG spectra are observed, while for $\phi = \pi/2$ there is sometimes only a single plateau in each HHG spectrum [cf. Figs. 3(d)-(f)]. We note that the shapes of the high-energy plateaus in Figs. 2 and 3 are sensitive to the partial (jth half-cycle) Keldysh parameters $\tilde{\gamma}_j$ [cf. Eq. (58) and Table I]. In particular, for the low-frequency case: (i) two-plateau structures are observed even for the sine-like ($\phi = \pi/2$) pulse [cf. Figs. 2(e)-(f)]; and (ii) additional bump-like structures can appear beyond the second plateau cutoff [cf. Figs. 2(d)-(e)]. Such crucial dependence of the shapes of HHG spectra on the laser parameters (e.g., CEP, wavelength, and pulse envelope) can be clearly explained in the framework of the present analytic theory, as we show in the following three sub-sections.

B. Sub-cycle and inter-cycle interferences in short-pulse HHG spectra

To understand the interference features of the short-pulse HHG spectra, it is necessary to examine the role of

TABLE I. Numerical values of $\mathcal{I}_j$ (75), $E_{\rm cut}^{(j)}$ (74), and $\tilde{\gamma}_j$ (58) for three half-cycles in Figs. 2(b) and 2(e). $|E_0| = 13.605\,$eV.

$\phi = 0$				$\phi = \pi/2$			
j	$\mathcal{I}_j$	$E_{\rm cut}^{(j)}$ (eV)	$\tilde{\gamma}_j$	j	$\mathcal{I}_j$	$E_{\rm cut}^{(j)}$ (eV)	$\tilde{\gamma}_j$
2	5.76(-9)	228.8	0.50	2	6.35(-7)	272.8	0.38
3	5.40(-6)	284.8	0.32	3	1.25(-5)	260.2	0.30
4	1.18(-5)	207.5	0.30	4	4.47(-6)	143.6	0.33

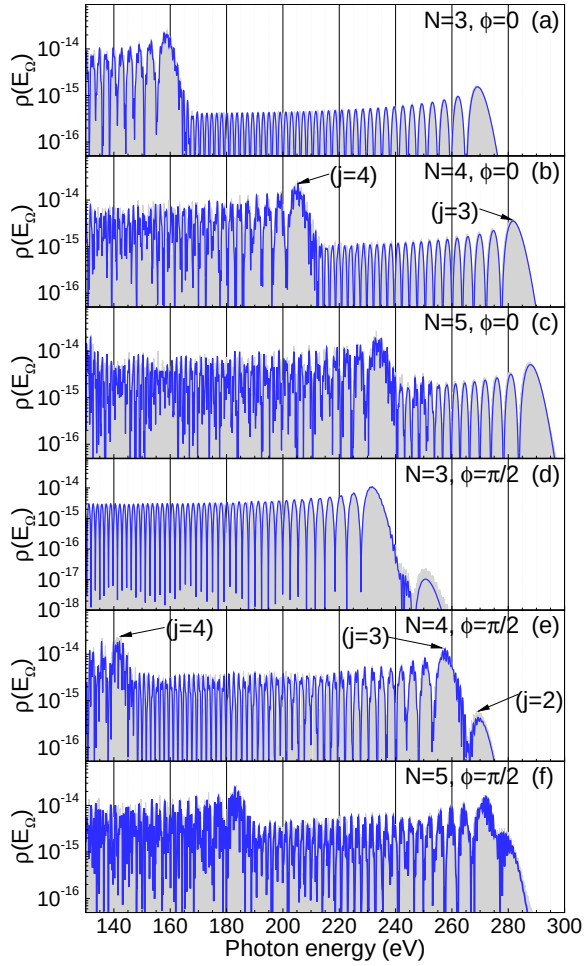

FIG. 2. (Color Online) HHG spectra of the H-atom for a $\sin^2$-shaped pulse [cf. Eq. (83)] with peak intensity $I = 10^{14}\,\mathrm{W/cm^2}$ and $\lambda = 3.1\,\mu$m. Grey area: Spherical coordinate TDSE results (see text); Solid (blue) lines: analytic results using Eq. (78). Results are given for three values of N, the number of cycles per pulse, and two values of the CEP, ϕ, as shown in each panel. Arrows mark the positions of $E_{\rm cut}^{(j)}$ [cf. Eq. (74)] given in Table I for three half cycles j.

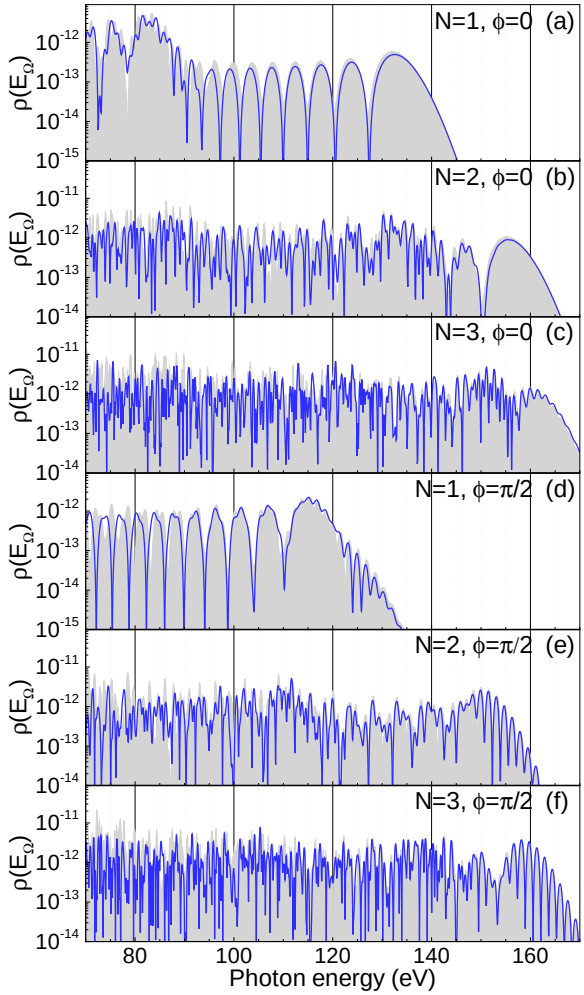

FIG. 3. (Color Online) The same as in Fig. 2, but for a Gaussian pulse [cf. Eq. (84] with $I = 2\times10^{14}\,\mathrm{W/cm^2}$ and $\lambda = 1.6\,\mu$m. Grey area: Cylindrical coordinate TDSE results (see text).

the various contributions to the spectra. The contribution of a partial wave packet w_j to the total HHG amplitude is governed by both the ionization [cf. Eq. (75)] and the propagation [cf. Eq. (72)] factors. However, the ionization factor determines only the magnitude of w_j and does not depend on the harmonic energy E_Ω. Its value depends only on the ionization potential $|E_0|$ and the electric field $\tilde{F}_j$ at the moment of ionization [in fact, this field is close to the maximum value of $F(t)$ during the jth half-cycle]. In the contrast, the propagation factor depends essentially on E_Ω: this factor oscillates for $E_\Omega < E_{\rm cut}^{(j)}$ and decreases exponentially in the region beyond the cutoff, $E_\Omega > E_{\rm cut}^{(j)}$, where the cutoff energy for the jth half-cycle is given by Eq. (74). If for a given laser pulse there are only a few half-cycles with large values of $E_{\rm cut}^{(j_i)}$, but for which $E_{\rm cut}^{(j_1)}$ is considerably larger than $E_{\rm cut}^{(j_2)}$ while $\tilde{F}_{j_1} < \tilde{F}_{j_2}$, and $E_{\rm cut}^{(j_2)} > E_{\rm cut}^{(j_3)}$ but $\tilde{F}_{j_2} < \tilde{F}_{j_3}$, and so on, then a multi-plateau structure is formed in the high-energy part of the HHG spectrum owing to the absence of overlapping partial HHG amplitudes, A_j. In Table I we present the three largest values of $E_{\rm cut}^{(j)}$ together with the ionization factors $\mathcal{I}_j$ and the effective Keldysh parameters $\tilde{\gamma}_j$ for the laser parameters applicable to the results in Figs. 2(b) and 2(e). For the cosine-pulse ($\phi = 0$) results in Fig. 2(b), the partial amplitude for $j = 2$ is suppressed relative to the partial amplitudes with $j = 3$ and $j = 4$ owing to the smallness of the ionization factor $\mathcal{I}_2$, while for the sine-pulse ($\phi = \pi/2$) results in Fig. 2(e) the contributions from all three half-cycles (with $j = 2$, 3, 4) are clearly visible.

The difference in HHG spectra for cosine-like ($\phi = 0$) and sine-like ($\phi = \pi/2$) pulses is clearly seen in Figs. 2 and 3: for $\phi = 0$, high energy plateaus exhibit large scale oscillations [cf. Figs. 2(a), 3(a)], while for $\phi = \pi/2$ these oscillations are modulated by fine-scale oscillations

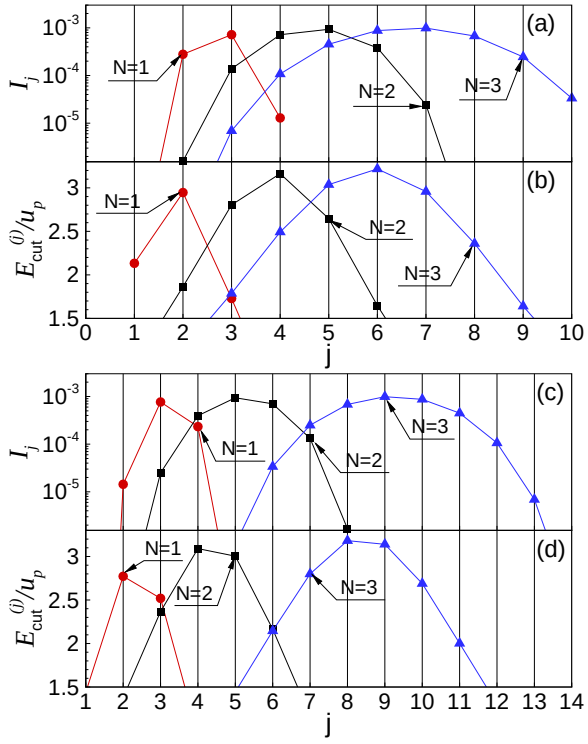

FIG. 4. (Color Online) Dependence of ionization factors $\mathcal{I}_j$ (75) and cutoff energies $E_{\rm cut}^j$ (74) on the half-cycle number j for laser parameters as in Fig. 3. Panels (a,b): $\phi = 0$; panels (c,d): $\phi = \pi/2$. Red lines with circles: $N = 1$; Black lines with squares: $N = 2$; Blue lines with triangles: $N = 3$.

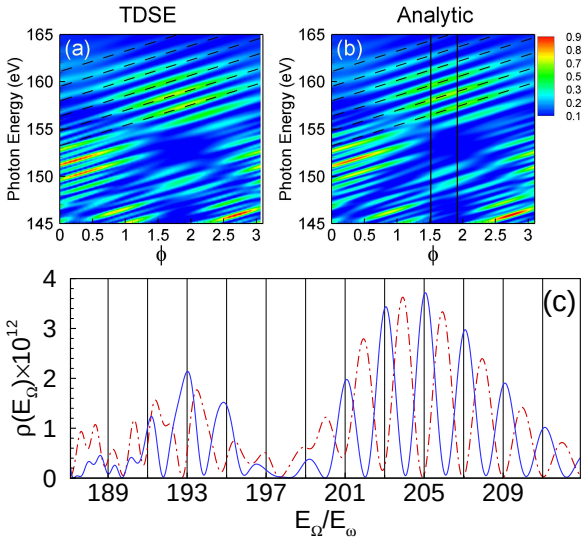

FIG. 5. (Color Online) Spectral density $\rho(E_\Omega, \phi)$ for the H atom and the same Gaussian pulse parameters (I, λ, N) as for Fig. 3(c). *Panels (a) and (b)*: Planar maps of $\rho(E_\Omega, \phi)$ (normalized relative to its maximum value) in the (E_Ω, ϕ) plane, with numerical TDSE results in (a) and analytic results of Eq. (78) in (b); dashed lines indicate the HHG "stripes" discussed in the text. *Panel (c)*: absolute analytic results for $\rho(E_\Omega, \phi)$ vs. relative energy E_Ω/E_ω (where $E_\omega = \hbar\omega$) plotted along the two solid vertical lines in (b), marking two fixed CEPs: $\phi = 1.51$ (dot-dashed line) and $\phi = 1.92$ (solid line).

[cf. Figs. 2(f) and 3(d)]. The origin of the large-scale oscillations is the same as for a monochromatic field [25], i.e., these oscillations originate from the interference of long and short electron trajectories for a given jth half-cycle and are described by the Airy function in Eq. (72). The fine-scale modulations originate from interference between different amplitudes $\mathcal{A}_j$; they are described by the term $w_{\rm int}$ in Eq. (82) [22]. This term simplifies when the interference of only two neighboring amplitudes in $w_{\rm int}$ is significant:

$$w_{\rm int} \approx 2 s_{j_1,j_2} \sqrt{w_{j_1} w_{j_2}} \cos(\varphi_{j_1} - \varphi_{j_2}). \qquad (85)$$

Equations (85) and (55) allow one to estimate the distance, ΔE_Ω, between two adjacent fine-scale peaks as the distance over which the phase difference in Eq. (85) changes by 2π:

$$\Delta E_\Omega = \frac{2\pi\hbar}{\Delta t_r^{(j)}}, \qquad (86)$$

where $\Delta t_r^{(j)}$ is the difference between recombination times for two [$(j+1)$th and jth] neighboring half-cycles: $\Delta t_r^{(j)} = t_r^{(j+1)} - t_r^{(j)}$. (Since $t_r^{(k)} \sim \omega^{-1}$, ΔE_Ω is of order $\hbar\omega$.) For a single-cycle ($N = 1$) cosine-like pulse, the fine-scale interference pattern appears in the region of the first plateau [cf. Fig. 3(a)] since it originates from the interference of amplitudes A_j with $j = 2$ and $j = 3$ [as is clear from Figs. 4(a),(b)]. For $E_\Omega > E_{\rm cut}^{(j=3)}$, the interference term $w_{\rm int}$ is negligible since the partial EWP $w_{j=3}$ decreases exponentially with increasing E_Ω and thus fine-scale oscillations disappear. The fine-scale interferences are pronounced for the sine-like pulse for $N = 1$ [cf. Fig. 3(d)] because there are two neighboring half-cycles with close values of both $E_{\rm cut}^{(j)}$ and $\mathcal{I}_j$, as shown in Figs. 4(c),(d) (i.e., for $N = 1$, half-cycles with $j = 2$ and 3 contribute to $w_{\rm int}$). With increasing N, the results for both cosine and sine-like pulses exhibit fine-scale modulation patterns in the cutoff region.

C. Dependence of quasi-harmonic structures in short-pulse HHG spectra on the CEP

The most prominent feature visible in Figs. 3(c) – 3(f) is the formation of quasi-harmonic patterns in the dependence of $\rho(E_\Omega)$ on E_Ω in the cutoff region and beyond. In previous studies [12, 13, 16, 18, 21] (see also Ref. [64]) these structures have been attributed to the real (but shifted) HHG peaks. However, our analytic results show that these structures have no relation whatsoever to the usual $2\hbar\omega$-spaced HHG peaks typical of a monochromatic driving laser field. Rather, these structures originate from the interference of two neighboring half-cycle HHG amplitudes, A_j. In Fig. 5 we show the variation of such

quasi-harmonic patterns in the cutoff and beyond-cutoff region as a function of the CEP, ϕ, for a Gaussian pulse with $N = 3$. Comparison of the planar maps of the spectral density $\rho(E_\Omega, \phi)$ in Figs. 5(a) and (b) shows that predictions of our analytic formula, Eq. (78), are in perfect agreement with numerical TDSE results over the entire range of CEPs, ϕ. Remarkably, as shown in Fig. 5(c), the positions of the "quasi-harmonics" can be tuned to either even or odd integers of the carrier frequency ω by varying the CEP [13, 15]. Moreover, in the plane (E_Ω, ϕ), intercycle interference causes the appearance of parallel stripes in the planar maps of spectral density $\rho(E_\Omega, \phi)$ in the high-energy part of the HHG spectra [cf. the dashed lines in Figs. 5(a) and (b)] [65]. Along the direction of these stripes, the value of $\rho(E_\Omega, \phi)$ varies slowly, while in the perpendicular direction its value oscillates. In order to understand this peculiar interference feature, we analyzed the dependence of various classical quantities (such as the ionization and recombination times, the classical action of an electron in a laser pulse, etc.) on the CEP using the numerical solutions of the classical equations (56) and (57). This analysis shows that for any pulse shape both ionization and recombination times depend linearly on the CEP ϕ [$\omega t_{i,r}^{(j)}(\phi) \approx \omega t_{i,r}^{(j)}(\phi_0) + \phi_0 - \phi$, where ϕ_0 is any phase from 0 to ϕ], in agreement with the same dependence of ionization and recombination times for the case of a monochromatic field [cf. Eq. (88) below].

Although the phases φ_j in Eq. (55) are nonlinear functions of ϕ, nevertheless, their difference, $\varphi_j - \varphi_i$ [which enters Eq. (85)], can be well approximated by a linear function of ϕ for energies near the cutoff, so that the interference term (85) can be approximated with high accuracy by:

$$w_{\rm int} \approx 2\sqrt{w_{j_1} w_{j_2}} \cos(\alpha E_\Omega + \beta\phi + \gamma), \qquad (87)$$

where α, β and γ are constants independent of E_Ω and ϕ. Considering $\rho(E_\Omega, \phi)$ along the line $\alpha E_\Omega + \beta\phi + \gamma = 2n\pi$ for a fixed integer n, we maximize the interference term and, as a result, the spectral density has maximal values along these lines. In the contrast, moving in the direction perpendicular to the stripes, the argument of the cosine in Eq. (87) changes continuously, so that the interference term $w_{\rm int}$ varies between its maximum and minimum values, leading to corresponding maxima and minima (i.e., quasi-harmonic patterns) in $\rho(E_\Omega, \phi)$.

D. Evolution of HHG spectra with increasing pulse duration

With increasing pulse duration, the number of half-cycles that contribute to the interference term $w_{\rm int}$ (82) for a given harmonic energy, E_Ω, increases gradually and leads to some unexpected interference patterns. For instance, for a Gaussian pulse with $N = 10$ the interference of many half-cycle amplitudes A_j leads to the appearance of an $\hbar\omega$-spaced HHG spectrum (cf. Fig. 6 for $\phi = 0.25$).

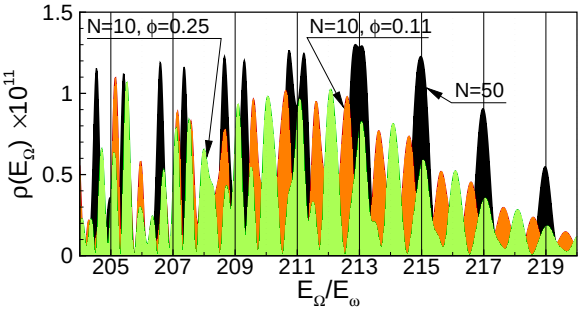

FIG. 6. (Color Online) Spectral density distribution $\rho(E_\Omega, \phi)$ vs. E_Ω/E_ω ($E_\omega = \hbar\omega$) in the plateau cutoff region for a Gaussian pulse with peak intensity $\mathrm{I} = 2\times10^{14}$ W/cm^2, carrier wavelength $\lambda = 1.6\,\mu$m, N optical cycles (FWHM), and CEP ϕ. Green (light grey) curve: $N = 10$, $\phi = 0.25$; orange (dark grey) curve: $N = 10$, $\phi = 0.11$; black curve: $N = 50$ (no dependence on ϕ).

As discussed above, the energy positions of such quasi-harmonics may be tuned by varying ϕ: for example, in Fig. 6 the green (light grey) curves with $\phi = 0.25$ have peaks at integer values of E_Ω/E_ω while the orange (dark grey) curves with $\phi = 0.11$ have peaks at half-integer values. The customary HHG peaks (i.e., $2\hbar\omega$-spaced peaks located at odd integer values of $\hbar\omega$, independent of ϕ) begin to form in the beyond-cutoff region for large N, as shown by the black curve for $N = 50$ in Fig. 6.

The case of a monochromatic laser field (whose entire HHG spectrum is comprised of a sequence of $2\hbar\omega$-spaced, CEP-independent peaks located at odd integer values of $\hbar\omega$) is obtained by taking the limit $\tau \to \infty$ (or $N \to \infty$) in our analytic results. In this limit, the vector potential $A(t)$ can be approximated by that of a monochromatic field and Eqs. (56) and (57) have the solution:

$$\begin{aligned} \omega t_i^{(j)} &= \tau_i - \phi + j\pi, \\ \omega t_r^{(j)} &= \tau_r - \phi + j\pi, \end{aligned} \qquad (88)$$

where $\tau_i \approx -2.83$ and $\tau_r \approx 1.26$. Since each half cycle is the same [except for the sign of $A(t)$ and $F(t)$], $\chi_\tau^{(j)} = \chi_\tau^{(k)}$, $\chi_w^{(j)} = \chi_w^{(k)}$, and $\varphi_j - \varphi_k = \pi(j-k)E_\Omega/(\hbar\omega)$ [cf. Eq. (55)]. Substituting these results in Eqs. (53), (54) and (24), we obtain:

$$\rho(E_\Omega) = \frac{\pi\Omega}{2\omega^2} W(E)\sigma^{(r)}(E) D(n, \Omega), \qquad (89)$$

where $W(E)$ is the EWP for a monochromatic field [25], n is the number of half-cycles ($n = 2N$), and

$$D(n, \Omega) = \left| \sum_{j=1}^{n} (-1)^j e^{i\pi j \frac{\Omega}{\omega}} \right|^2 = \left(\frac{\sin\frac{1}{2}nx}{\sin\frac{1}{2}x} \right)^2, \qquad (90)$$

where

$$x = \pi\left(\frac{\Omega}{\omega} - 1\right).$$

For $N \to \infty$, $D(n,\Omega)$ becomes a sum of δ-functions [66]:

$$D(n,\Omega)\Big|_{n\gg 1} \to \frac{2\omega^2}{\pi} T_N \sum_k \delta[\Omega-(2k+1)\omega], \qquad (91)$$

where T_N is the pulse duration: $T_N = 2\pi N/\omega$. For a long pulse, it is useful to introduce the power of emitted radiation, $\mathcal{W}_{\rm tot}$, i.e., the ratio of total energy radiated during the pulse, $\mathcal{E}_{\rm tot}$, to pulse duration:

$$\mathcal{W}_{\rm tot} = \lim_{N\to\infty} \mathcal{E}_{\rm tot}/T_N. \qquad (92)$$

Substituting Eq. (91) into Eq. (89) and integrating the latter over E_Ω, we obtain the total power, $\mathcal{W}_{\rm tot}$, as:

$$\mathcal{W}_{\rm tot} = \sum_k \mathcal{W}_{2k+1}, \quad \mathcal{W}_{2k+1} = (2k+1)\hbar\omega \mathcal{R}_{2k+1}, \quad (93)$$

where the partial power of the $(2k+1)$th harmonic ($\mathcal{W}_{2k+1}$) is expressed in terms of the HHG rate $\mathcal{R}_{2k+1}$ for the $(2k+1)$th harmonic [25, 42].

The above analysis shows that our analytical results for short pulses uniformly approach those for a monochromatic laser field in the limit that the pulse duration becomes infinitely long. We emphasize that it is the interference term, $w_{\rm int}$, that is responsible for the formation of $2\hbar\omega$-spaced HHG peaks (located at odd-integer multiples of the carrier frequency) as the number of optical cycles, N, in the pulse becomes large. For a given pulse shape, the monochromatic field limit is reached when: (i) The magnitudes of the half-cycle amplitudes, A_j, are close in value to each other; and (ii) The phase differences between the half-cycle amplitudes are essentially independent of the peak intensity. These two conditions can only be satisfied simultaneously for quasi-monochromatic pulses. However, the critical number of optical cycles, $N_{\rm cr}$, at which a stable shape (i.e., independent of the CEP, ϕ) of the HHG spectrum begins to form in the cutoff energy region, depends crucially on both the shape of the laser pulse and its peak intensity, I. For instance, for a trapezoidal pulse, $N_{\rm cr} \sim 3$ and the shape of the HHG spectrum is only slightly sensitive to the intensity, I. For this reason, a trapezoidal pulse shape is the most appropriate one for analyzing the monochromatic field limit. In contrast, for Gaussian pulses, $N_{\rm cr}$ depends significantly on the intensity: e.g., $N_{\rm cr} \sim 40$ for $I = 4\times10^{14}$ W/cm^2, ~ 15 for $I = 2\times10^{14}$ W/cm^2 (cf. Fig. 7), and ~ 10 for $I = 10^{14}$ W/cm^2.

Finally, we remark that our analytical description provides a remarkably clear illustration of how the regular ($2\hbar\omega$-spaced) feature of HHG spectra begins to form (with increasing number N of optical cycles) from the often complicated spectral structure of short-pulse HHG radiation. Since for small N the inter-cycle interferences are highly sensitive to the CEP, as shown in Fig. 6, the evolution of these interferences with increasing N can best be seen by considering spectra that are averaged over the CEP. In Fig. 7 we present such CEP-averaged spectral densities $\rho(E_\Omega)$ for the same Gaussian pulse as

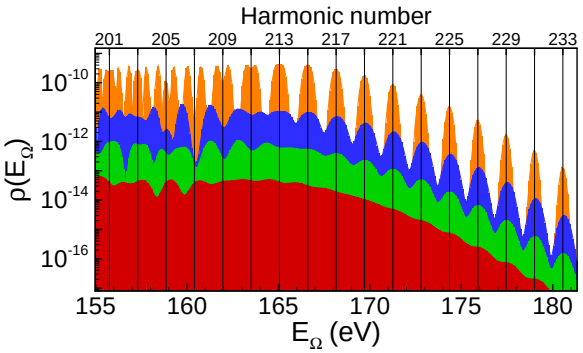

FIG. 7. (Color Online) CEP-averaged spectral density distribution $\rho(E_\Omega)$ (not normalized, for better visualization) in the plateau cutoff region and beyond for different numbers N of optical cycles (FWHM) in the same Gaussian pulse as in Fig. 6. The numbers N of cycles for the four filled areas [from bottom (red) to top (orange)] are: $N = 10$, 15, 20, and 40.

in Fig. 6 for four values of N, from 10 to 40. Such averaging smooths out the fine scale-oscillations for $N = 10$ (seen in Fig. 6 for two values of the CEP). Such averaging, however, is less significant for $N = 15$ or 20, and beginning from $N = 40$, the results do not depend on ϕ. As shown in Fig. 7, a stable harmonic structure gradually appears with increasing N beginning for energies E_Ω well beyond the plateau-cutoff energy, with the first signature of this structure appearing for $N = 10$ as horizontal steps centered close to the positions of odd harmonics, $E_\Omega = (2k+1)\hbar\omega$. For larger N, the regular structure becomes more distinct and extends toward the plateau cutoff position (corresponding to the 213th harmonic) with gradually increasing peak heights and narrowing peak widths centered at the odd-harmonic energies. Such evolution of the short-pulse HHG spectrum is not surprising. Indeed, with increasing N, the half-cycle ionization factors $\mathcal{I}_j$ (which do not depend on the harmonic energy E_Ω and which determine the absolute values of both the partial EWPs w_j and the amplitudes A_j) become independent of the half-cycle number j. However, condition (ii) (cf. prior paragraph) for the phase difference, $\Delta_{jk} = \phi_j - \phi_k$, between half-cycle amplitudes A_j and A_k is fulfilled for energies E_Ω primarily beyond the plateau-cutoff. This is because in this region the first (linear in E_Ω) term in Eq. (55) for ϕ_j exceeds the second (intensity and CEP-dependent) term, allowing the realization of the condition $\Delta_{jk} = (t_r^{(j)} - t_r^{(k)})E_\Omega/\hbar \approx \pi(j-k)E_\Omega/(\hbar\omega)$ that is necessary for "constructive" interference of half-cycle HHG amplitudes at odd integers of the ratio $E_\Omega/(\hbar\omega)$ [cf. Eq. (90)]. The results in Fig. 7, which employ a Gaussian approximation for the pulse envelope, are useful for understanding qualitatively the evolution of short-pulse HHG spectra with increasing N. However, as N increases this approximation becomes inappropriate because a flat-top envelope is more relevant for long pulses. In this case, the regular HHG spectrum is formed for a much smaller N than for a Gaussian pulse. Indeed, our analysis for a

trapezoidal pulse shape finds that the formation of a $2\hbar\omega$-spaced HHG spectrum over a wide interval of harmonic energy E_Ω occurs already for $N = 5$.

VII. SUMMARY AND CONCLUSIONS

In this work we have derived quantum-mechanically closed-form analytical formulas for the spectral density $\rho(E_\Omega, \phi)$ of coherent radiation emitted by an atomic system subjected to an intense, short laser pulse with CEP ϕ. Our main results consist, first, in generalizing our TDER theory [36, 37] (for describing a weakly bound electron in a short-range potential subjected to an intense, monochromatic laser field) to the case of an intense, few-cycle laser pulse. The key idea is to treat the case of an infinitely long pulse train of short laser pulses and then to take the limit that the time between pulses becomes infinite. We then derive closed-form analytic expressions for the spectral density $\rho(E_\Omega, \phi)$ of generated radiation by a few-cycle laser pulse that include the dependence on the number of cycles N in the pulse and on the CEP ϕ of the pulse. The resulting formulas factorize into factors corresponding to the three steps of the well-known three-step scenario [10, 11]. These formulas also confirm the phenomenological parametrization [26–28] of the HHG yield in terms of the PRCS $\sigma^{(r)}$ (which describes the final step of the three-step scenario) and the EWP (which describes the ionization of an atomic electron and its propagation in the laser field). Most importantly, we provide a closed-form expression for the EWP factor for the case of a few-cycle laser pulse. Moreover, we generalize the analytic formulas derived for our TDER model system to treat HHG by real atoms in a few-cycle laser pulse.

Our analytic formulas show that the spectral density $\rho(E_\Omega, \phi)$ is highly sensitive to both the CEP, ϕ, and the number of optical cycles, N, in the pulse. The fine-scale oscillation pattern of the HHG plateau near the high energy cutoff is shown to originate from interference between EWPs ionized from a few neighboring half-cycles in the vicinity of the peak of the laser pulse intensity envelope. Moreover, the CEP, ϕ, can be used to tune the energy locations of peaks in the plateau spectrum of $\rho(E_\Omega, \phi)$. Only in the limit that $N \to \infty$ does the interference pattern become the one expected for a monochromatic laser field: harmonics separated in energy by $2\hbar\omega$ and located at odd integer values of the carrier frequency, ω. The closed form analytic formula derived for our TDER model system was easily generalized to describe HHG by real atoms owing to the transparent physical meaning of each of the three factors of which it is comprised. This formula is thus applicable for describing HHG by atoms in a few-cycle laser pulse provided only that the intensity and carrier frequency of the pulse lie in the tunneling regime.

We conclude by emphasizing the valuable insight into strong field processes provided by closed-form analytic formulas. Although such formulas can be derived only for model systems and/or within limited ranges of the laser parameters, they allow one to obtain a detailed understanding of the underlying physics applicable to real systems. We note, finally, that ours is not the only theory capable of providing closed-form analytic formulas for strong field processes. Recently, O.I. Tolstikhin, T. Morishita, and S. Watanabe presented a general adiabatic theory of ATI and applied this theory to the case of a one-dimensional zero-range-potential model [67]. This work obtained a factorized analytic formula describing ATI for that model that is consistent with the suggested factorization proposed in Ref. [26] and is applicable in the limit that the driving laser period is long compared to electronic time scales in atoms. Various details of the simple model system treated in Ref. [67] differ from those of our three-dimensional TDER model system that was applied in Ref. [55] for analytic description of ATI in a monochromatic laser field. However, the advantage of such analytical approaches is that (in addition to the physical insight they provide) the closed form formulas provide experimentalists with the means both to plan experiments and to probe any differences between results of different theoretical models.

ACKNOWLEDGMENTS

We acknowledge T.S. Sarantseva for useful discussions. This work was supported by RFBR Grants Nos. 10-02-00235, 10-02-01250, and 11-02-00064, by NSF Grant No. PHY-0901673, by the Ministry of Education and Science of the Russian Federation, and by the "Dynasty" Foundation (A.A.S). Calculations at MSU were performed on the SKIF "Chebyshev" supercomputer.

Appendix A: Derivation of Eqs. (43) and (44)

To evaluate $\mathcal{I}'_{F_h}(E_0, 0)$ in Eq. (42), we express the integral (40) in an alternative form. Using the definition (31) for $\tilde{\mathcal{G}}_\varepsilon(t, t')$ and proceeding as in Ref. [68], the integrand of Eq. (40) can be written as a sum of two terms,

$$\frac{e^{i\tilde{k}_n|\mathcal{R}(t,t')|} - 1}{|\mathcal{R}(t,t')|} = \frac{\cos\tilde{k}_n|\mathcal{R}(t,t')| - 1}{|\mathcal{R}(t,t')|} + i\frac{\sin[\tilde{k}_n\mathcal{R}(t,t')]}{\mathcal{R}(t,t')}, \tag{A1}$$

where the first term on the right is an even function of $\tilde{k}_n$, while the second term is odd. Expanding the even term in a series in $\tilde{k}_n$ [cf. Eq. (35)] and substituting this expansion into the integral (40), the contribution of the $\tilde{k}_n$-even term becomes:

$$\mathcal{I}_e = \iint_{-\mathcal{T}/2}^{\mathcal{T}/2} \sum_n \sum_{\nu=1}^{\infty} \frac{(-1)^\nu \tilde{k}_n^{2\nu} g_\nu(t,t') e^{-in\omega_\tau(t-t')}}{(2\nu)!!} dt dt',$$

$$g_\nu(t,t') = |\mathcal{R}(t,t')|^{2\nu-1} \exp\left\{-\frac{i}{\hbar}\int_{t'}^{t}\left[\frac{e^2\mathcal{A}^2(\tau)}{2mc^2} - \tilde{u}_p\right]d\tau\right\},$$

where $g_\nu(t,t') \sim |t-t'|^{2\nu-1}$ at $t \to t'$. Using the definition of $\tilde{k}_n$ in Eq. (35), the integral $\mathcal{I}_e$ becomes:

$$\mathcal{I}_e = \mathcal{T}\sum_{\nu=1}^{\infty}\sum_{s=0}^{\nu}\iint_{-\mathcal{T}/2}^{\mathcal{T}/2}\frac{(-1)^{\nu+s}C_{2\nu}^{s}(\varepsilon-\tilde{u}_p)^{\nu-s}}{(2\nu)!!} \times(i\hbar)^s\delta^{(s)}(t-t')g_\nu(t,t')dtdt', \quad \text{(A2)}$$

where $C_{2\nu}^{s}$ is a binomial coefficient and $\delta^{(s)}(t-t')$ is the s-fold derivative of the δ-function in the space of periodic functions:

$$\delta^{(s)}(t-t') = \sum_n (-in\omega_\tau)^s e^{-in\omega_\tau(t-t')}. \quad \text{(A3)}$$

Using Eq. (A3), the integrations in Eq. (A2) can be performed straightforwardly and show that $\mathcal{I}_e = 0$.

The integral (40) thus simplifies upon substituting,

$$\frac{e^{i\tilde{k}_n|\mathcal{R}(t,t')|}-1}{|\mathcal{R}(t,t')|} \to \frac{e^{i\tilde{k}_n\mathcal{R}(t,t')}-e^{-i\tilde{k}_n\mathcal{R}(t,t')}}{2\mathcal{R}(t,t')}, \quad \text{(A4)}$$

and representing the integral $\mathcal{I}(\varepsilon,F_h)$ as a summation over simpler integrals $\mathcal{I}_n$:

$$\mathcal{I}(\varepsilon,F_h) = \frac{1}{2\kappa\mathcal{T}^2}\sum_{n=-\infty}^{\infty}\mathcal{I}_n, \quad \text{(A5)}$$

$$\mathcal{I}_n = \iint_{-\mathcal{T}/2}^{\mathcal{T}/2}\frac{e^{-i\mathcal{S}_n^-(t,t')/\hbar}-e^{-i\mathcal{S}_n^+(t,t')/\hbar}}{\mathcal{R}(t,t')}dtdt', \quad \text{(A6)}$$

where $\mathcal{S}_n^\pm(t,t')$ is the classical action:

$$\mathcal{S}_n^\pm(t,t') = \int_{t'}^{t}\left[\frac{[\mathcal{P}_n^\pm(t'')]^2}{2m}-\varepsilon\right]dt'', \quad \text{(A7)}$$

$$\mathcal{P}_n^\pm(t) = \tilde{p}_n \pm \frac{|e|}{c}\mathcal{A}(t), \quad \tilde{p}_n = \hbar\tilde{k}_n. \quad \text{(A8)}$$

To extract explicitly the linear in F_h result in the expansion of $\mathcal{I}(\varepsilon,F_h)$ in the limit $F_h \to 0$, we transform first the expression (A6) for $\mathcal{I}_n$ (presenting it as $\mathcal{I}_n = \mathcal{I}_n^- - \mathcal{I}_n^+$) as follows:

$$\mathcal{I}_n^\pm \equiv \iint_{-\mathcal{T}/2}^{\mathcal{T}/2}\frac{e^{-i\mathcal{S}_n^\pm(t,t')/\hbar}}{\mathcal{R}(t,t')}dtdt' = \iint_{-\mathcal{T}/2}^{\mathcal{T}/2}\frac{e^{-i\mathcal{S}_n^\pm(t,t')/\hbar}\left(\alpha\frac{\partial\mathcal{S}_n^\pm}{\partial t}+\beta\frac{\partial\mathcal{S}_n^\pm}{\partial t'}\right)}{\mathcal{R}(t,t')\left(\alpha\frac{\partial\mathcal{S}_n^\pm}{\partial t}+\beta\frac{\partial\mathcal{S}_n^\pm}{\partial t'}\right)}dtdt' = i\hbar\alpha\iint_{-\mathcal{T}/2}^{\mathcal{T}/2}\frac{d[e^{-i\mathcal{S}_n^\pm(t,t')/\hbar}]dt'}{\mathcal{R}(t,t')\left(\alpha\frac{\partial\mathcal{S}_n^\pm}{\partial t}+\beta\frac{\partial\mathcal{S}_n^\pm}{\partial t'}\right)} + i\hbar\beta\iint_{-\mathcal{T}/2}^{\mathcal{T}/2}\frac{dtd[e^{-i\mathcal{S}_n^\pm(t,t')/\hbar}]}{\mathcal{R}(t,t')\left(\alpha\frac{\partial\mathcal{S}_n^\pm}{\partial t}+\beta\frac{\partial\mathcal{S}_n^\pm}{\partial t'}\right)}, \quad \text{(A9)}$$

where α and β are free parameters. [Note that the derivatives, $\partial\mathcal{S}_n^\pm/\partial t$ or $\partial\mathcal{S}_n^\pm/\partial t'$, of the function $\mathcal{S}_n^\pm(t,t')$ depend only on the single variable, t or t', respectively.]

Next, we integrate by parts in Eq. (A9), keeping only terms of the lowest order in $1/\mathcal{R}$, to obtain

$$\mathcal{I}_n^\pm \approx i\hbar\alpha^2\iint_{-\mathcal{T}/2}^{\mathcal{T}/2}\frac{e^{-i\mathcal{S}_n^\pm(t,t')/\hbar}\frac{\partial^2\mathcal{S}_n^\pm}{\partial t^2}dtdt'}{\mathcal{R}(t,t')\left(\alpha\frac{\partial\mathcal{S}_n^\pm}{\partial t}+\beta\frac{\partial\mathcal{S}_n^\pm}{\partial t'}\right)^2} + i\hbar\beta^2\iint_{-\mathcal{T}/2}^{\mathcal{T}/2}\frac{e^{-i\mathcal{S}_n^\pm(t,t')/\hbar}\frac{\partial^2\mathcal{S}_n^\pm}{\partial t'^2}dtdt'}{\mathcal{R}(t,t')\left(\alpha\frac{\partial\mathcal{S}_n^\pm}{\partial t}+\beta\frac{\partial\mathcal{S}_n^\pm}{\partial t'}\right)^2}. \quad \text{(A10)}$$

Finally, we use the saddle point method to estimate the integral over t' in the first term in Eq. (A10) and that over t in the second term. The derivative $\partial\mathcal{S}_n^\pm/\partial t'$ ($\partial\mathcal{S}_n^\pm/\partial t$) in the denominator of the first (second) integral in Eq. (A10) becomes zero since it determines the corresponding saddle point equation. Thus the free parameters α and β do not enter the final result for $\mathcal{I}_n$:

$$\begin{aligned}\mathcal{I}_n \approx{}& i\hbar\sum_\nu\sqrt{\frac{2\pi i\hbar}{\mathcal{S}_n^{-\prime\prime}(t_\nu^-)}}\int_{-\mathcal{T}/2}^{\mathcal{T}/2}\frac{e^{-i\mathcal{S}_n^-(t,t_\nu^-)/\hbar}\mathcal{S}_n^{-\prime\prime}(t)}{\mathcal{R}(t,t_\nu^-)[\mathcal{S}_n^{-\prime}(t)]^2}dt \\ &-i\hbar\sum_\nu\sqrt{\frac{2\pi i\hbar}{\mathcal{S}_n^{+\prime\prime}(t_\nu^+)}}\int_{-\mathcal{T}/2}^{\mathcal{T}/2}\frac{e^{-i\mathcal{S}_n^+(t,t_\nu^+)/\hbar}\mathcal{S}_n^{+\prime\prime}(t)}{\mathcal{R}(t,t_\nu^+)[\mathcal{S}_n^{+\prime}(t)]^2}dt \\ &-i\hbar\sum_\nu\sqrt{\frac{2\pi\hbar}{i\mathcal{S}_n^{-\prime\prime}(t_\nu^{-*})}}\int_{-\mathcal{T}/2}^{\mathcal{T}/2}\frac{e^{-i\mathcal{S}_n^-(t_\nu^{-*},t')/\hbar}\mathcal{S}_n^{-\prime\prime}(t')}{\mathcal{R}(t_\nu^{-*},t')[\mathcal{S}_n^{-\prime}(t')]^2}dt' \\ &+i\hbar\sum_\nu\sqrt{\frac{2\pi\hbar}{i\mathcal{S}_n^{+\prime\prime}(t_\nu^{+*})}}\int_{-\mathcal{T}/2}^{\mathcal{T}/2}\frac{e^{-i\mathcal{S}_n^+(t_\nu^{+*},t')/\hbar}\mathcal{S}_n^{+\prime\prime}(t')}{\mathcal{R}(t_\nu^{+*},t')[\mathcal{S}_n^{+\prime}(t')]^2}dt',\end{aligned} \quad \text{(A11)}$$

where

$$\mathcal{S}_n^{\pm\prime}(t) = \frac{[\mathcal{P}_n^\pm(t)]^2}{2m}-\epsilon, \quad \text{(A12)}$$

$$\mathcal{S}_n^{\pm\prime\prime}(t) = \mp\frac{|e|}{m}\mathcal{P}_n^\pm(t)\mathcal{F}(t). \quad \text{(A13)}$$

The saddle point equations for $t_\nu^\pm$ are:

$$\frac{[\mathcal{P}_n^\pm(t_\nu^\pm)]^2}{2m} = E_0, \quad \text{(A14)}$$

where ε is approximated by E_0, and $t_\nu^\pm$ are the roots of Eq. (A14) for which the imaginary parts of $\mathcal{S}_n^{\pm\prime\prime}(t_\nu^\pm)$ are positive.

Consider first the *imaginary* part of $\mathcal{I}$ for *real* $\epsilon < 0$ [to which only open n-photon ATI channels contribute, as follows from (A6)]. Its expression in terms of $\mathcal{I}_n$ is:

$$\tilde{\mathcal{I}} \equiv i\mathrm{Im}\mathcal{I}(\varepsilon,F_h) = \frac{\mathcal{I}-\mathcal{I}^*}{2} = \frac{1}{2\kappa\mathcal{T}^2}\sum_{n>n_0}\mathcal{I}_n, \quad \text{(A15)}$$

where $n_0 = [(\tilde{u}_p-\epsilon)/(\hbar\omega)]$ (where $[x]$ is the integer part of x) and $\tilde{u}_p$ is defined by Eq. (34). Assuming $\hbar\Omega \gg |E_0|$, we can neglect in Eq. (A11) for $\mathcal{I}_n$ any dependence of $\mathcal{P}_n^\pm$, $\mathcal{S}_n^\pm$, $\mathcal{S}_n^{\pm\prime}$, $\mathcal{R}$, and the saddle points $t_\nu^\pm$ on F_h in the limit $F_h \to 0$, other than that stemming from the terms $\mathcal{F}(t)$ and $\mathcal{F}(t')$ in the derivatives $\mathcal{S}_n^{\pm\prime\prime}(t)$

and $\mathcal{S}_n^{\pm\prime\prime}(t')$ [cf. Eq. (A13)] in the numerators of the integrals in Eq. (A11). Thus the linear in F_h term in the expansion of $\mathcal{I}_n$ in F_h follows only from the linear dependence of $\mathcal{F}(t)$ on F_h [cf. Eq. (28)] in Eq. (A13) for these derivatives. Hence, the derivative (in F_h) of $\tilde{\mathcal{I}}$ is obtained as:

$$\tilde{\mathcal{I}}'_{F_h} \equiv \frac{\partial\tilde{\mathcal{I}}}{\partial F_h}\Big|_{F_h=0} = e^{i\phi_h}\Phi_\Omega + e^{-i\phi_h}\Phi_{-\Omega}, \tag{A16}$$

where

$$\begin{aligned}\Phi_{\pm\Omega} = {}& \frac{i\hbar|e|}{4m\kappa\mathcal{T}^2}\sum_{n>n_0}^{\infty}\sum_{\nu} \\ & \sqrt{\frac{2\pi i\hbar}{S_n^{-\prime\prime}(t_\nu^-)}}\int_{-\mathcal{T}/2}^{\mathcal{T}/2}\frac{e^{-iS_n^-(t,t_\nu^-)/\hbar\pm i\Omega t}P_n^-(t)}{R(t,t_\nu^-)\left[\frac{[P_n^-(t)]^2}{2m}-E_0\right]^2}dt \\ & +\sqrt{\frac{2\pi i\hbar}{S_n^{+\prime\prime}(t_\nu^+)}}\int_{-\mathcal{T}/2}^{\mathcal{T}/2}\frac{e^{-iS_n^+(t,t_\nu^+)/\hbar\pm i\Omega t}P_n^+(t)}{R(t,t_\nu^+)\left[\frac{[P_n^+(t)]^2}{2m}-E_0\right]^2}dt \\ & -\sqrt{\frac{2\pi\hbar}{iS_n^{-\prime\prime}(t_\nu^{-*})}}\int_{-\mathcal{T}/2}^{\mathcal{T}/2}\frac{e^{-iS_n^-(t_\nu^{-*},t)/\hbar\pm i\Omega t}P_n^-(t)}{R(t_\nu^{-*},t)\left[\frac{[P_n^-(t)]^2}{2m}-E_0\right]^2}dt \\ & -\sqrt{\frac{2\pi\hbar}{iS_n^{+\prime\prime}(t_\nu^{+*})}}\int_{-\mathcal{T}/2}^{\mathcal{T}/2}\frac{e^{-iS_n^+(t_\nu^{+*},t)/\hbar\pm i\Omega t}P_n^+(t)}{R(t_\nu^{+*},t)\left[\frac{[P_n^+(t)]^2}{2m}-E_0\right]^2}dt,\end{aligned} \tag{A17}$$

and definitions of $S_n^\pm(t,t')$, $P_n^\pm(t)$, and $R(t,t')$ are given by Eqs. (A7) (with $\varepsilon = E_0$), (A8), and (32) with $F_h = 0$, while $t_\nu^\pm$ are given by Eq. (A14) with $\mathcal{P}_n^\pm \to P_n^\pm$. Moreover, since Eq. (A17) involves only integrals over the period $\mathcal{T}$, the vector potential $A_\tau(t)$ can be replaced by $A(t)$ in these integrals [cf. Eq. (4)].

Since $\tilde{\mathcal{I}}$ determines only the imaginary part of $\mathcal{I}$ [cf. Eq. (A15)], to find an explicit form for $\mathcal{I}'_{F_h}(E_0,0)$ in Eq. (42), it is necessary to express Eq. (A16) for $\tilde{\mathcal{I}}'_{F_h}$ as a difference of two terms similar to that of $\mathcal{I}-\mathcal{I}^*$ in Eq. (A15). For this purpose, we separate the saddle points $t_\nu^\pm$ in the integrals for Φ_Ω in Eq. (A17) into two groups:

(i) Saddle points from the first group satisfy the equation:

$$p_n \pm A(t_{1,\nu}^\pm) = -i\hbar\kappa, \tag{A18}$$

where we label those as $t_{1,\nu}^\pm$; and

(ii) Saddle points from the second group (labeled as $t_{-1,\nu}^\pm$) satisfy the equation:

$$p_n \pm A(t_{-1,\nu}^\pm) = +i\hbar\kappa. \tag{A19}$$

The solutions of (A18) and (A19) are related as follows:

$$t_{1,\nu}^\pm = [t_{-1,\nu}^\pm]^*. \tag{A20}$$

To separate the contributions of these two groups of saddle points to Φ_Ω in Eq. (A17), we re-write Φ_Ω as

$$\Phi_\Omega = \Phi_\Omega^{(1)} + \Phi_\Omega^{(-1)}, \tag{A21}$$

where $\Phi_\Omega^{(j)}$ corresponds to the $j=\pm1$ saddle point group:

$$\begin{aligned}\Phi_\Omega^{(j)} = {}& \frac{i\hbar|e|}{4m\kappa\mathcal{T}^2}\sum_{\sigma=\pm1}\sum_{n>n_0}^{\infty}\sum_{\nu}\sqrt{\frac{2\pi m\,\sigma j}{\mu_{j,\nu}^\sigma|e|F(t_{j,\nu}^\sigma)\kappa}} \\ & \times\int_{-\mathcal{T}/2}^{\mathcal{T}/2}\frac{e^{-i\mu_{j,\nu}^\sigma S_n^\sigma(t,t_{j,\nu}^\sigma)/\hbar+i\Omega t}P_n^\sigma(t)}{R(t,t_{j,\nu}^\sigma)\left[\frac{[P_n^\sigma(t)]^2}{2m}-E_0\right]^2}dt,\end{aligned} \tag{A22}$$

where $\mu_{j,\nu}^\sigma = \pm1$ is the sign of the imaginary part of the saddle point $t_{j,\nu}^\sigma$. [Eq. (A22) follows from Eq. (A17), taking into account Eqs. (A13), (A18), (A19), and (A20).] Though saddle points with both positive and negative parts contribute to Eq. (A22), the contributions of those with $\mathrm{Im}\,t_{j,\nu}^\sigma < 0$ are negligible for $\Omega > |E_0|$. Indeed, the saddle points of the integrand in Eq. (A22) satisfy:

$$\mu_{j,\nu}^\sigma\left(\frac{[P_n^\sigma(t)]^2}{2m}-E_0\right) = \hbar\Omega. \tag{A23}$$

For $\mu_{j,\nu}^\sigma = -1$ and $\Omega > |E_0|$, the saddle points are complex, so that the corresponding integrals are small, whereas for $\mu_{j,\nu}^\sigma = 1$ the saddle points are real and the integrals are not small. Thus we substitute $\mu_{j,\nu}^\sigma = +1$ and neglect contributions of saddle points with $\mathrm{Im}\,t_{j,\nu}^\sigma < 0$.

¿From the symmetry relation (A20) and the explicit form (A22) for $\Phi_\Omega^{(j)}$, it follows that

$$\Phi_\Omega^{(1)} = -\Phi_{-\Omega}^{(-1)*}. \tag{A24}$$

This symmetry relation allows us to write $\tilde{\mathcal{I}}'_{F_h}$ as:

$$\tilde{\mathcal{I}}'_{F_h} = \frac{\mathcal{I}'_{F_h} - \mathcal{I}'^*_{F_h}}{2}, \tag{A25}$$

where

$$\mathcal{I}'_{F_h} = 2\left(\Phi_\Omega^{(1)}e^{i\phi_h} + \Phi_{-\Omega}^{(1)}e^{-i\phi_h}\right). \tag{A26}$$

Finally, from Eqs. (A25), (A26), and (A15), we obtain:

$$4C_{\kappa\,0}^2|E_0|\mathcal{I}'_{F_h}(E_0,0) = \tilde{\mathcal{D}}_\Omega e^{i\phi_h} + \tilde{\mathcal{D}}_{-\Omega}e^{-i\phi_h}, \tag{A27}$$

where the HHG amplitude, $\tilde{\mathcal{D}}_\Omega = 8C_{\kappa\,0}^2|E_0|\Phi_\Omega^{(1)}$, is given by Eqs. (44) – (48).

Appendix B: Analytic estimates of the HHG amplitude for a short laser pulse

To simplify the result (51) for the HHG amplitude in the low-frequency limit ($\hbar\omega \ll |E_0|$), we estimate the integral over p by the saddle point method. The saddle point $p = \tilde{p}$ and the second derivative of the classical action $S(t,t_\nu^\sigma;p)$ in Eq. (47) at $p=\tilde{p}$ are given by:

$$\begin{aligned}&\tilde{p} = \sigma q, \quad q = -\frac{|e|}{c}\frac{\int_{t_\nu^\sigma}^t A(\tau)d\tau}{t-t_\nu^\sigma}, \\ &\frac{\partial^2 S}{\partial p^2}\Big|_{p=\tilde{p}} = \frac{t-t_\nu^\sigma}{m} + i\frac{\hbar\kappa}{m}\frac{\partial t_\nu^\sigma(p)}{\partial p}\Big|_{p=\tilde{p}} \approx \frac{t-t_\nu^\sigma}{m},\end{aligned} \tag{B1}$$

so that the saddle-point result for $\tilde{\mathcal{D}}(t)$ is:

$$\tilde{\mathcal{D}}(t) = |e|\kappa^{-1} \sum_{\sigma=\pm 1} \tilde{d}_\sigma(t), \tag{B2}$$

$$\tilde{d}_\sigma(t) = \sum_\nu f_{\nu,\sigma}(t) \frac{e^{-i\tilde{S}(t,t_\nu^\sigma)/\hbar}\tilde{P}(t)}{\left[\frac{\tilde{P}(t)^2}{2m} - E_0\right]^2}, \tag{B3}$$

where

$$f_{\sigma,\nu}(t) = C_{\kappa 0}^2 |E_0| \sigma \sqrt{\frac{\hbar}{i\kappa|e|\sigma F(t_\nu^\sigma)(t-t_\nu^\sigma)^3}},$$
$$\tilde{P}(t) = \frac{|e|}{c}\left[A(t) - \frac{1}{t-t_\nu^\sigma}\int_{t_\nu^\sigma}^t A(\tau)d\tau\right],$$
$$\tilde{S}(t,t_\nu) = \int_{t_\nu^\sigma}^t \left[\frac{[q+\frac{|e|}{c}A(\tau)]^2}{2m} - E_0\right] d\tau, \tag{B4}$$

and the equation for the saddle points t_ν^σ $[= t_\nu^\sigma(t)]$ follows from Eq. (49) upon substituting there $p_n \to \tilde{p}$:

$$\frac{|e|}{c}\left[A(t_\nu^\sigma) - \frac{1}{t-t_\nu^\sigma}\int_{t_\nu^\sigma}^t A(\tau)d\tau\right] = -i\sigma\hbar\kappa. \tag{B5}$$

To estimate the integral over t in Eq. (50) for $\tilde{\mathcal{D}}(\Omega)$, we use the techniques suggested in Ref. [69] for evaluating integrals involving functions with two close (nearly equal) saddle points, as used recently in Refs.[31, 42] (cf. also Ref. [70]). Briefly, for the integral in Eq.(50), one expands $\tilde{S}(t,t_\nu^\sigma)$ in (B3) in powers of t (up to the cubic term) about the point $\overline{t}_\nu^\sigma$ at which the second derivative of $\tilde{S}$ is zero, and then evaluates the integral in terms of Airy functions, $\mathrm{Ai}(x)$.

Double differentiation of $\tilde{S}(t,t_\nu^\sigma)$ in Eq. (B4) yields the equation for $\overline{t}_\nu^\sigma$:

$$\frac{F(t_\nu^\sigma)\tilde{P}(t)}{|e|F(t_\nu^\sigma)(t-t_\nu^\sigma) - i\sigma\hbar\kappa} - F(t) = 0, \tag{B6}$$

where $t = \overline{t}_\nu^\sigma$. To evaluate $\tilde{\mathcal{D}}(\Omega)$, we substitute (B2) and (B3) in (50) and, taking into account the equation for the saddle points of the function $\exp\{-i[\tilde{S}(t,t_\nu^\sigma)/\hbar - \Omega t]\}$,

$$\tilde{P}(t) = \sqrt{2mE}, \quad E = \hbar\Omega + E_0, \tag{B7}$$

remove the pre-exponent from the integrand in the integral over t upon substituting there $\tilde{P}(t) \to \sqrt{2mE}$, $(t - t_\nu^\sigma) \to (\overline{t}_\nu^\sigma - t_\nu^\sigma)$. Then, after approximating $\tilde{S}$ in (B3) by the cubic polynomial in t, we obtain for $\tilde{\mathcal{D}}(\Omega)$:

$$\begin{aligned}\tilde{\mathcal{D}}(\Omega) &\approx \frac{e\kappa^{-1}}{\pi}\frac{\sqrt{2mE}}{(E-E_0)^2}\sum_{\sigma,\nu} f_{\sigma,\nu}\int_{-\infty}^{\infty} e^{-i\tilde{S}(t,t_\nu^\sigma)/\hbar + i\Omega t}dt \\ &\approx \frac{e\kappa^{-1}}{\pi}\frac{\sqrt{2mE}}{(E-E_0)^2}\sum_{\sigma,\nu} f_{\sigma,\nu} e^{-i\tilde{S}_\nu^\sigma/\hbar + i\Omega\overline{t}_\nu^\sigma} \\ &\times \int_{-\infty}^{\infty} e^{i(E-\mathcal{E}_{\sigma,\nu})(t-\overline{t}_\nu^\sigma)/\hbar + \zeta_{\sigma,\nu}(t-\overline{t}_\nu^\sigma)^3/(3\hbar^3)}dt \\ &= 2e\kappa^{-1}\frac{\sqrt{2mE}\hbar}{(E-E_0)^2}\sum_{\sigma,\nu}\frac{f_{\sigma,\nu}e^{-i\tilde{S}_\nu^\sigma/\hbar + i\Omega\overline{t}_\nu^\sigma}}{\zeta_{\sigma,\nu}^{1/3}}\mathrm{Ai}\left(\xi_{\sigma,\nu}\right),\end{aligned} \tag{B8}$$

where we have introduced the notations: $\tilde{S}_\nu^\sigma \equiv \tilde{S}(\overline{t}_\nu^\sigma, t_\nu^\sigma)$, $f_{\sigma,\nu} \equiv f_{\sigma,\nu}(\overline{t}_\nu^\sigma)$, and

$$\xi_{\sigma,\nu} = \frac{E - \mathcal{E}_{\sigma,\nu}}{\zeta_{\sigma,\nu}^{1/3}}, \tag{B9}$$

$$\mathcal{E}_{\sigma,\nu} = \frac{e^2}{2mc^2}\left[A(\overline{t}_\nu^\sigma) - \frac{\int_{t_\nu^\sigma}^{\overline{t}_\nu^\sigma} A(\tau)d\tau}{\overline{t}_\nu^\sigma - t_\nu^\sigma}\right]^2, \tag{B10}$$

$$\begin{aligned}\zeta_{\sigma,\nu} = \frac{e\hbar^2\tilde{P}(\overline{t}_\nu^\sigma)}{2m}\Bigg\{&-\dot{F}(t_\nu^\sigma)\left[\frac{F(\overline{t}_\nu^\sigma)}{F(t_\nu^\sigma)}\right]^2\left(1-\mathcal{L}^{-1}\right) \\ &+\frac{F(\overline{t}_\nu^\sigma)\left[\frac{1}{c}\frac{A(\overline{t}_\nu^\sigma)-A(t_\nu^\sigma)}{\overline{t}_\nu^\sigma - t_\nu^\sigma} + F(t_\nu^\sigma)\right]}{F(t_\nu^\sigma)(\overline{t}_\nu^\sigma - t_\nu^\sigma)\mathcal{L}^2} + \dot{F}(\overline{t}_\nu^\sigma)\Bigg\},\end{aligned} \tag{B11}$$

$$\mathcal{L} = 1 + \frac{i\sigma\hbar\kappa}{|e|F(t_\nu^\sigma)(\overline{t}_\nu^\sigma - t_\nu^\sigma)}. \tag{B12}$$

Further simplification of the complicated general result (B8) that allows for a better physical interpretation follows by using an approximate solution of the basic Eqs. (B5) and (B6) for the times t_ν^σ and $\overline{t}_\nu^\sigma$. Both t_ν^σ and $\overline{t}_\nu^\sigma$ are complex owing to the terms $\sim \hbar\kappa$, which have a quantum origin (cf. Ref. [42]). As for the case of a monochromatic field [42], for an intense, low-frequency pulse field $F(t)$ with vector potential (52), the quantum term $i\sigma\hbar\kappa$ in (B5) and (B6) can be treated iteratively. In our case, this means that the "effective Keldysh parameter", $\tilde{\gamma} = \hbar\omega/(|e|\tilde{F}\kappa^{-1})$ [where $\tilde{F}$ is a characteristic value of the field $F(t)$], is small: $\tilde{\gamma} \ll 1$. In the tunnel limit ($\tilde{\gamma} \to 0$), (B5) and (B6) reduce to the classical equations,

$$A(t_i^{(\nu)}) - \frac{1}{t_r^{(\nu)} - t_i^{(\nu)}}\int_{t_i^{(\nu)}}^{t_r^{(\nu)}} A(\tau)d\tau = 0, \tag{B13}$$

$$\frac{1}{c}\frac{A(t_r^{(\nu)}) - A(t_i^{(\nu)})}{t_r^{(\nu)} - t_i^{(\nu)}} + F(t_r^{(\nu)}) = 0, \tag{B14}$$

for closed classical trajectories of an electron in the field $\mathbf{F}(t)$, along which an electron with zero velocity at the initial (ionization) time $t_i \equiv t_i^{(\nu)}$ gains the maximum kinetic energy from the field $\mathbf{F}(t)$ at the final (recombination) time $t_r \equiv t_r^{(\nu)}$. We consider only classically-allowed

closed trajectories, for which t_i and t_r are real and the return time is smaller than the optical period of the pulse, i.e., $(t_r - t_i) < 2\pi/\omega$. For a short pulse (52) involving N optical cycles of frequency ω, the index ν enumerates the ionization ($t_i^{(\nu)}$) and recombination ($t_r^{(\nu)}$) times for the νth *half-cycle* [where $t_r^{(\nu)}$ lies in the $(\nu+1)$th half-cycle].

The solution of Eqs. (B5) and (B6), taking account of the quantum terms $\sim \hbar\kappa$ perturbatively, has the form:

$$t_\nu^\sigma \approx t_i - i\frac{\hbar\kappa}{|e|\tilde{F}(t_i)} + \delta t_i, \tag{B15}$$

$$\overline{t}_\nu^\sigma \approx t_r + \delta t_r, \tag{B16}$$

where

$$\tilde{F}(t_i) = \sigma F(t_i) > 0, \tag{B17}$$

$$\delta t_i = \frac{\hbar^2\kappa^2}{2e^2F(t_i)^2\Delta t}\left[1 + \frac{\dot{F}(t_i)}{F(t_i)}\Delta t + \frac{F(t_r)}{F(t_i)}\alpha\right], \tag{B18}$$

$$\delta t_r = \frac{\hbar^2\kappa^2\alpha}{2e^2F(t_i)^2\Delta t}, \tag{B19}$$

$$\alpha = \frac{1 - \frac{F(t_i)}{F(t_r)} - \frac{\dot{F}(t_i)}{F(t_i)}\Delta t}{1 - \frac{F(t_r)}{F(t_i)} + \frac{\dot{F}(t_r)}{F(t_r)}\Delta t}, \tag{B20}$$

$$\Delta t = t_r - t_i. \tag{B21}$$

With the use of expansions (B15) and (B16), all parameters in the expression (B8) for $\tilde{\mathcal{D}}(\Omega)$ can be presented in terms of the classical times t_i and t_r. Numerically, the quantum corrections in Eq. (B11) for $\zeta_{\sigma,\nu}$ are found to be negligible, so that we can make the approximations

$$\zeta_{\sigma,\nu} \approx -E_{\rm at}^3\zeta_\nu,$$
$$\zeta_\nu = -\frac{I(t_r)}{2I_{\rm at}}\left[1 - \frac{F(t_r)}{F(t_i)} + \frac{\dot{F}(t_r)}{F(t_r)}\Delta t\right], \tag{B22}$$

where $I(t_r) = cF(t_r)^2/(8\pi)$, $I_{\rm at} = 3.51\times10^{16}$ W/cm^2, and $E_{\rm at} = 27.21$ eV. In the expansion for the energy $\mathcal{E}_{\sigma,\nu}$ [cf. Eq. (B10)], we take into account the first quantum correction (which is of order $\hbar^2\kappa^2 \sim |E_0|$), to obtain

$$\mathcal{E}_{\sigma,\nu} \approx E_{\rm max} = \mathcal{E}_{\rm max}^{\rm cl}(t_i, t_r) - \frac{F(t_r)}{F(t_i)}|E_0|, \tag{B23}$$

where

$$\mathcal{E}_{\rm max}^{\rm cl}(t_i, t_r) = \frac{e^2}{2mc^2}\left[A(t_r) - A(t_i)\right]^2. \tag{B24}$$

Taking into account the results (B22) and (B23), we obtain for the argument $\xi_{\sigma,\nu}$ of the Airy function in (B8):

$$\xi_{\sigma,\nu} \approx \xi = \frac{E - E_{\rm max}}{\zeta_\nu^{1/3}E_{\rm at}}. \tag{B25}$$

The expansion of the classical action $\tilde{S}_\nu^\sigma$ in (B8) involves an imaginary term stemming from $\mathrm{Im}\, t_\nu^\sigma$ [cf. Eq. (B15)]:

$$\tilde{S}_\nu^\sigma \approx S_0 = \int_{t_i}^{t_r}\left[\mathcal{E}_{\rm max}^{\rm cl}(t_i, t) - E_0\right]dt + \mathcal{E}_{\rm max}^{\rm cl}(t_i, t_r)\Delta t - i\frac{2}{3}\frac{\hbar\kappa|E_0|}{|e|\tilde{F}(t_i)}. \tag{B26}$$

Since the last term in (B26) involves $\hbar\kappa|E_0| \sim (\hbar\kappa)^3$, it would seem that the term involving Δt should also be expanded up to terms of order $(\hbar\kappa)^3$. However, we find that these latter corrections give such a small contribution that they may be neglected.

Substituting Eqs. (B8), (B22), (B25), and (B26) into Eq. (50), we obtain the HHG amplitude in the form (53), in which we use the summation index j (instead of ν) for enumerating the solutions $(t_i^{(j)}, t_r^{(j)})$ of the classical equations (B13) and (B14).

[1] P.B. Corkum and F. Krausz, Nat. Phys. **3**, 381 (2007).
[2] F. Krausz and M. Ivanov, Rev. Mod. Phys. **81**, 163 (2009).
[3] M. Nisoli and G.Sansone, Prog. Quantum Electron. **33**, 17 (2009).
[4] F. Ferrari, F. Calegari, M. Lucchini, C. Vozzi, S. Stagira, G. Sansone, and M. Nisoli, Nat. Phot. **4**, 875 (2010).
[5] G. Sansone, L. Poletto, and M. Nisoli, Nat. Phot. **5**, 655 (2011).
[6] T. Popmintchev, M.-C. Chen, P. Arpin, M.M. Murnane, and H.C. Kapteyn, Nat. Phot. **4**, 822 (2010).
[7] T. Brabec and F. Krausz, Rev. Mod. Phys. **72**, 545 (2000).
[8] P. Agostini and L.F. DiMauro, Rep. Prog. Phys. **67**, 813 (2004).
[9] A. Scrinzi, M.Yu. Ivanov, R. Kienberger, and D.M. Villeneuve, J. Phys. B **39**, R1 (2006).
[10] K.J. Schafer, B. Yang, L.F. DiMauro, and K.C. Kulander, Phys. Rev. Lett. **70**, 1599 (1993).
[11] P.B. Corkum, Phys. Rev. Lett. **71**, 1994 (1993).
[12] A. de Bohan, P. Antoine, D.B. Milošević, and B. Piraux, Phys. Rev. Lett. **81**, 1837 (1998).
[13] A. Baltuška, T. Udem, M. Uiberacker, M. Hentschel, E. Goulielmakis, C. Gohle, R. Holzwarth, V. S. Yakovlev, A. Scrinzi,T. W. Hansch, and F. Krausz, Nature (London) **421**, 611 (2003).
[14] V.S. Yakovlev and A. Scrinzi, Phys. Rev. Lett. **91**, 153901 (2003).
[15] M. Nisoli, G. Sansone, S. Stagira, S. De Silvestri, C. Vozzi, M. Pascolini, L. Poletto, P. Villoresi, and G. Tondello, Phys. Rev. Lett. **91**, 213905 (2003).
[16] G. Sansone, C. Vozzi, S. Stagira, and M. Nisoli, Phys. Rev. A **70**, 013411 (2004).
[17] G. Sansone, E. Benedetti, J.-P. Caumes, S. Stagira, C.

Vozzi, S. De Silvestri, and M. Nisoli, Phys. Rev. A **73**, 053408 (2006).
[18] C.A. Haworth, L.E. Chipperfield, J.S. Robinson, P.L. Knight, J.P. Marangos, and J.W.G. Tisch, Nat. Phys. **3**, 52 (2007).
[19] A.D. Bandrauk, S. Chelkowski, D.J. Diestler, J. Manz, and K.-J. Yuan, Phys. Rev. A **79**, 023403 (2009).
[20] P. Huang, X.-T. Xie, X. Lü, J. Li, and X. Yang, Phys. Rev. A **79**, 043806 (2009).
[21] G. Sansone, E. Benedetti, J.P. Caumes, S. Stagira, C. Vozzi, M. Nisoli, L. Poletto, P. Villoresi, V. Strelkov, I. Sola, L.B. Elouga, A. Zaïr, E. Mével, and E. Constant, Phys. Rev. A **80**, 063837 (2009).
[22] M.V. Frolov, N.L. Manakov, A.A. Silaev, N.V. Vvedenskii, and A.F. Starace, Phys. Rev. A **83**, 021405(R) (2011).
[23] F. Calegari, M. Lucchini, K.S. Kim, F. Ferrari, C. Vozzi, S. Stagira, G. Sansone, and M. Nisoli, Phys. Rev. A **84**, 041802(R) (2011).
[24] M. Lewenstein, Ph. Balcou, M.Y. Ivanov, A. L'Huillier, and P.B. Corkum, Phys. Rev. A **49**, 2117 (1994).
[25] M.V. Frolov, N.L. Manakov, T.S. Sarantseva, M.Yu. Emelin, M.Yu. Ryabikin, and A.F. Starace, Phys. Rev. Lett. **102**, 243901 (2009).
[26] T. Morishita, A.T. Le, Z. Chen, and C.D. Lin, Phys. Rev. Lett. **100**, 013903 (2008).
[27] A.T. Le, T. Morishita, and C. D. Lin, Phys. Rev. A **78**, 023814 (2008).
[28] C.D. Lin, A.T. Le, Z. Chen, T. Morishita, and R. Lucchese, J. Phys. B **43**, 122001 (2010).
[29] S. Minemoto, T. Umegaki, Y. Oguchi, T. Morishita, A.T. Le, S. Watanabe, and H. Sakai, Phys. Rev. A **78**, 061402(R) (2008).
[30] H.J. Wörner, H. Niikura, J.B. Bertrand, P.B. Corkum, and D.M. Villeneuve, Phys. Rev. Lett. **102**, 103901 (2009).
[31] M.V. Frolov, N.L. Manakov, A.A. Silaev, N.V. Vvedenskii, Phys. Rev. A **81**, 063407 (2010)
[32] M.V. Frolov, N.L. Manakov, and A.F. Starace, Phys. Rev. A **82**, 023424 (2010).
[33] A.D. Shiner, B.E. Schmidt, C. Trallero-Herrero, H.J. Wörner, S. Patchkovskii, P.B. Corkum, J.-C. Kieffer, F. Légaré, and D.M. Villeneuve, Nat. Phys. **7**, 464 (2011).
[34] R.A. Ganeev, L.B. Elouga Bom, J.-C. Kieffer, and T. Ozaki, Phys. Rev. A **75**, 063806 (2007).
[35] R.A. Ganeev, M. Suzuki, M. Baba, and H. Kuroda, Phys. Rev. A **76**, 023805 (2007).
[36] M.V. Frolov, N.L. Manakov, E.A. Pronin, and A.F. Starace, Phys. Rev. Lett. **91**, 053003 (2003).
[37] M.V. Frolov, N.L. Manakov, and A.F. Starace, Phys. Rev. A **78**, 063418 (2008).
[38] M.V. Frolov, N.L. Manakov, E.A. Pronin, and A.F. Starace, J. Phys. B **36**, L419 (2003).
[39] I.Yu. Kiyan and H. Helm, Phys. Rev. Lett. **90**, 183001 (2003).
[40] M.V. Frolov, A.V. Flegel, N.L. Manakov, and A.F. Starace, Phys. Rev. A **75**, 063407 (2007).
[41] M.V. Frolov, A.V. Flegel, N.L. Manakov, and A.F. Starace, Phys. Rev. A **75**, 063408 (2007).
[42] M.V. Frolov, N.L. Manakov, T.S. Sarantseva, and A.F. Starace, J. Phys. B **42**, 035601 (2009).
[43] D.B. Milošević, G.G. Paulus, D. Bauer, and W. Becker, J. Phys. B **39**, R203 (2006).
[44] N.L. Manakov, V.D. Ovsiannikov, and L.P. Rapoport, Phys. Rep. **141**, 319 (1986).
[45] N.L. Manakov, M.V. Frolov, B Borca, and A.F. Starace, J. Phys. B **36**, R49 (2003).
[46] M.V. Frolov, A.A. Khuskivadze, N.L. Manakov, and A.F. Starace, J. Phys. B **39**, S283 (2006).
[47] N.L.Manakov, M.V. Frolov, A.F. Starace, and I.I. Fabrikant, J. Phys. B **33**, R141 (2000).
[48] R.M. Potvliege and R. Shakeshaft, Phys. Rev. A **40**, 3061 (1989).
[49] L.D. Landau and E.M. Lifshitz, *Quantum Mechanics* (Nonrelativistic Theory), 3rd ed. (Pergamon, Oxford, 1977).
[50] N.L. Manakov and A.G. Fainshtein, Teor. Mat. Fiz. **48**, 375 (1981) [Theor. Math. Phys. **48**, 815 (1982)].
[51] N.L. Manakov and A.G. Fainshtein, Zh. Eksp. Teor. Fiz. **79**, 751 (1980) [Sov. Phys. JETP **52**, 382 (1980)].
[52] M.Yu. Kuchiev and V.N. Ostrovsky, J. Phys. B **32**, L189 (1999); Phys. Rev. A **60**, 3111 (1999).
[53] L.V. Keldysh, Zh. Eksp. Teor. Fiz. **47**, 1945 (1964) [Sov. Phys. JETP **20**, 1307 (1965)].
[54] V.S. Popov, Pis'ma Zh. Eksp. Teor. Fiz. **73**, 3 (2001) [JETP Lett. **73**, 1 (2001)]; B.M. Karnakov, V.D. Mur, and V.S. Popov, Pis'ma Zh. Eksp. Teor. Fiz. **88**, 495 (2008) [JETP Lett. **88**, 423 (2008)].
[55] M.V. Frolov, N.L. Manakov, and A.F. Starace, Phys. Rev. A **79**, 033406 (2009).
[56] B.M. Smirnov and M.I. Chibisov, Zh. Eksp. Teor. Fiz. **49**, 841 (1965) [Sov. Phys. JETP **22**, 585 (1966)].
[57] M.V. Frolov, N. L. Manakov, T. S. Sarantseva, and A.F. Starace, Phys. Rev. A **83**, 043416 (2011).
[58] I.I. Sobel'man, *Introduction to the Theory of Atomic Spectra* (Elsevier, Oxford, 1972).
[59] I.A. Burenkov, A.M. Popov, O.V. Tikhonova, and E.A. Volkova, Laser Phys. Lett. **7**, 409 (2010).
[60] A.M. Popov, O.V. Tikhonova, and E.A. Volkova, Laser Phys. **21**, 1593 (2011).
[61] A.A. Silaev and N.V. Vvedenskii, Phys. Rev. Lett. **102**, 115005 (2009).
[62] A.A. Silaev and N.V. Vvedenskii, Phys. Scr. T **135**, 014024 (2009).
[63] J.L. Krause, K.J. Schafer, and K.C. Kulander, Phys. Rev. A **45**, 4998 (1992).
[64] E. Priori, G. Cerullo, M. Nisoli, S. Stagira, S. De Silvestri, P. Villoresi, L. Poletto, P. Ceccherini, C. Altucci, R. Bruzzese, and C. de Lisio, Phys. Rev. A **61**, 063801 (2000).
[65] G. Sansone, Phys. Rev. A **79**, 053410 (2009).
[66] P. Antosik, J. Mikusiński, and R. Sikorsky, *Theory of Distributions: The Sequential Approach* (Elsevier, Amsterdam, 1973) Chap. 1, Sec. 4.2.
[67] O.I. Tolstikhin, T. Morishita, and S. Watanabe, Phys. Rev. A **81**, 033415 (2010).
[68] I.J. Berson, J. Phys. B **8**, 3078 (1975).
[69] A.I. Nikishov and V.I. Ritus, Zh. Exp. Teor. Fiz. **46**, 776 (1964) [Sov. Phys. JETP **19**, 529 (1964)].
[70] S.P. Goreslavskii and S.V. Popruzhenko, J. Phys. B **32**, L531 (1999).